SUPPLEMENTAL MATERIAL

Splicing machinery is impaired in Rheumatoid Arthritis, associated with disease activity and modulated by Anti-TNF therapy

Alejandro Ibáñez-Costa[1]*, Carlos Perez-Sanchez[1]*, Alejandra M. Patiño-Trives[1]*, María Luque-Tévar[1], Pilar Font[1], Iván Arias de la Rosa[1], Cristobal Roman-Rodriguez[1], María Carmen Ábalos[1], Carmen Conde[2], Antonio González[2], Sergio Pedraza-Arévalo[3,4,5,6], Mercedes Del Río-Moreno[3,4,5,6], Ricardo Blazquez-Encinas[3,4,5,6], Pedro Segui[7], Jerusalem Calvo[1], Rafaela Ortega-Castro[1], Alejandro Escudero-Contreras[1], Nuria Barbarroja[1], M.ª Ángeles Aguirre[1], Justo P. Castaño[3,4,5,6], Raúl M. Luque[3,4,5,6], Eduardo Collantes[#1] and Chary López-Pedrera[#1].

Patients and Methods

Blood sample collection, assessment of clinical and biological parameters, and B-mode ultrasound IMT measurements.

Peripheral blood leukocyte subsets including monocytes, neutrophils and lymphocytes were isolated from the peripheral blood of RA patients and HD, using Ficoll Hypaque gradient and specific cell separation commercial kits (Miltenyi Biotech) and an autoMACS Pro Separator (Miltenyi Biotech, Bergisch Gladbach, Germany) as previously described.[14]

In a subset of patients from the first RA cohort, mononuclear cells were also collected from both, synovial fluid and peripheral blood by Ficoll Hypaque gradient to perform matching studies.

In the second cohort, comprising RA patients treated with anti-TNF, blood samples were obtained before and after 3 and 6 months of treatment. To avoid blood composition changes promoted by diet and circadian rhythms, samples were always collected in the early hours of the morning and after a fasting period of 8 hours.

Radiological involvement was assessed by evaluating the presence and number of eroded joints, joint space narrowing, soft tissue swelling, or joint effusion among other manifestations, such as osteoporosis or the presence of subcutaneous rheumatoid nodules.

Ibáñez-Costa A, *et al. Ann Rheum Dis* 2021; 81:56–67. doi: 10.1136/annrheumdis-2021-220308

B-Mode Ultrasound IMT Measurements

RA patients and controls underwent B-mode ultrasound imaging for carotid intimae media thickness (CIMT) measurements as previously described9. B-mode ultrasound imaging of the carotid arteries was performed by using Toshiba equipment (Aplio platform) equipped with 7–10 MHz broadband linear array transducers.

Patients were examined in the supine position, with the head turned 45° contralateral to the side of scanning. Three carotid arterial segments were assessed: the common carotid (1 cm proximal to the bulb), the carotid bulb (between the dilatation and flow divider), and the internal carotid (1 cm distal to the flow divider). Of each segment, the near and the far walls of the left and right carotid artery segments were imaged at 2 different angles. The maximum distance of the intima-media thickness, defined as "maximum IMT" was calculated for each view. The plaque was defined as a focal structure that encroached into the arterial lumen of at least 0.5 mm or 50% of the surrounding IMT value or demonstrated a thickness >1.5 mm as measured from the media-adventitia interface to the intima-lumen interface.

Analysis of splicing machinery components by qPCR dynamic array based on microfluidic technology

Total RNA from monocytes, neutrophils and lymphocytes was isolated using TRIsure (Bioline, Memphis, TX, USA) followed by a DNAse treatment (RQ1DNAse, Promega; Wisconsin, USA) ensuing manufacturer's instructions. RNA purity and concentration were evaluated using Nanodrop spectrophotometer (Thermo Scientific, Waltham, MA, USA). 1000 ng of total RNA were retrotranscribed using NZY Reverse Transcriptase kit (NZYTech, Lisboa, Portugal) using random hexamer primers. A 48.48 Dynamic Array (Fluidigm, San Francisco, CA, USA) was used to assess the expression of 45 selected transcripts of the major and minor spliceosome and associated splicing factors as previously reported.[12-16]

Fluidigm (South San Francisco, CA, USA) dynamic arrays use microfluidics [an "integrated fluidic circuit" (IFC) connected to reagent input wells] and high-resolution imaging to perform qPCR with fluorescence detection in nanoliter reaction volumes. This microfluidics system allows more rapid screening of large sample sets and

Ibáñez-Costa A, *et al. Ann Rheum Dis* 2021; 81:56–67. doi: 10.1136/annrheumdis-2021-220308

consumption of substantially lower amounts of PCR reagents, while avoiding the reaction-compatibility requirements of multiplex systems that combine several target detection assays in 1 reaction (J Biomol Tech. 2016 Jul; 27(2): 75–83. doi: 10.7171/jbt.16-2702-003).

The panel of splicing machinery components was selected on the basis of two main criteria: 1) the relevance of the given spliceosome components in the splicing process [such as the components of the spliceosome core (SNRNP70, RNU2, RNU4, RNU5, SNRNP200, U2AF1, U2AF2, SF3B1, TCERG1, PRPF40A, PRPF8, RBM22, RNU11, RNU12, RNU4ATAC, RNU6ATAC)], and 2) its demonstrated role in autoimmune, rheumatic or inflammatory diseases (NOVA1, PTBP1, RAVER1, RBM45, SFPQ, SND1, SNW1, SRSF1, SRSF2, SRSF5, TIA1).

In the present study, a 48.48 Dynamic Array based on microfluidic technology (Fluidigm, San Francisco, CA, USA) was implemented, to determine the expression of 48 transcripts in 48 samples, simultaneously. Specific primers for human transcripts including components of the major (n=13) and minor spliceosome (n=4), associated SFs (n=28) and three housekeeping genes were specifically designed with the Primer3 software and StepOne™ Real-Time PCR System software v2.3 (Applied Biosystems, Foster City, CA, USA). Following manufacturer's instructions, 12.5ng of cDNA of each sample were pre-amplified using 1µL of PreAmp Master Mix (Fluidigm) and 0.5µL of all primers mix (500nM) in a T100 Thermal-cycler (BioRad, Hercules, CA, USA), using the following program: 1) 2 min at 95ºC; 2) 15 sec at 94ºC and 4 min at 60ºC (14 cycles). Then, samples were treated with 2µL of 4U/µL Exonuclease I solution (New England BioLabs, Ipswich, MA, USA) following manufacturer's instructions. Then, samples were diluted with 18µL of TE Buffer (Thermo Scientific), and 2.7µL were mixed with 3µL of EvaGreen Supermix (Bio-Rad) and 0.3µL of DNA Binding Dye Sample Loading Reagent (Fluidigm). Primers were diluted to 5µM with 2X Assay Loading Reagent (Fluidigm). Control line fluid was charged in the chip and Prime script program was run into the IFC controller MX (Fluidigm). Finally, 5µL of each primer and 5µL of each sample were pipetted into their respective inlets on the chip and the Load Mix script in the IFC controller software was run. After this program, the qPCR was run in the Biomark System (Fluidigm) following the thermal cycling program: 1) 95ºC for 1min; 2) 35 cycles of denaturing (95ºC for 5sec) and annealing/extension (60ºC for 20sec); and 3) a last

cycle where final PCR products were subjected to graded temperature-dependent dissociation (60ºC to 95ºC, increasing 1ºC/3 sec).

Data were processed with Real-Time PCR Analysis Software 3.0 (Fluidigm).

Additionally, total RNA from PAXgene tubes containing whole blood samples, obtained from the second RA cohort involving patients treated with TNFi for six months, was purified by using the PAXgene Blood RNA kit (PreAnalytiX, Hombrechtikon, Switzerland).

Validation of altered spliceosome components in RA patients treated with TNFi and in HD treated with purified ACPA-IgG from RA patients or with non-immune IgG from HD was performed by quantitative real time PCR (qPCR) using LightCycler 480 (Applied Biosystems, Foster City, CA, USA) thermocycler and above-mentioned primers.

Bioplex assay of the inflammatory profile in plasma of RA patients

Secreted levels of 27 cytokines/chemokines/adhesion molecules in plasma of RA patients were determined using a 27-plex panel in a multiplex bead-based assay system (Bio-Plex multiplex immunoassays, Bio Rad; CA, USA). The assay was performed according to the manufacturer's protocol using Bio-Plex 200 system based on Luminex technology. Briefly, plasma samples were transferred to magnetic beads and incubated for 1 h at room temperature. After incubation, a series of steps including plate wash, antibody and streptavidin incubation before exposure of plate were performed. Finally, the samples were acquired and quantified using Bio-plex 200 (Luminex 200, USA). Cytokine concentrations were determined from standard curves prepared on each plate and expressed as pg/ml using the Bio-Plex ManagerTM software (Bio-Rad, Hercules, CA, USA).

Analysis of an external RNAseq dataset to validate gene expression and identify splicing variants.

RNA-seq data of an external cohort of 44 patients (E-MTAB-6141) was analyzed as validation cohort to explore gene expression and splicing profile. This dataset included matching data of whole blood cells and synovial biopsies.

Gene expression and splicing variants analysis.

Raw paired-end FASTQ files were trimmed using Trim Galore and quality check was assessed using Fast QC and normalized using Salmon and the last release (v34) of

human GENCODE transcriptome. The relative abundance of transcripts in transcripts per million (TPM) generated by Salmon were used as input for SUPPA2 software to perform the calculation of relative abundances of the splicing events as Percent Spliced In Index (PSI or Ψ). For differential expression analyses and to compare splicing variants considering high or low expression, gene abundances were imported to R and summarized to gene-level using Tximeta and normalized and quantified using DESeq2. In each comparison, samples were classified according to gene expression using third and first quartiles samples. PSI and TPM values for the low and high expression groups were used with SUPPA2 to perform the differential splicing analysis with local events, then splicing differences using delta PSI (ΔΨ) were calculated. The difference in average PSI from each group with adjusted, and p value < 0.05 were considered significant. The PSI values were used to calculate the relative frequency of each splicing event per sample [Relative Frequency (event i) = (Σ PSI (event i))/(Σ PSI (total events))] and estimate the splicing event composition per sample. The comparisons between high and low groups were tested by t test with significance cutoff at p < 0.05. Classification of splicing event profiling was established into 7 types of events according to their splicing pattern: alternative 3' splice site, alternative 5' splice site, alternative first exon, alternative last exon, mutually exclusive exons, retained intron and skipped exon.

Gene Ontology (GO) terms enrichment analyses were performed using DAVID online software v6.8, *(Huang Da W, Sherman BT, Lempicki RA. Systematic and integrative analysis of large gene lists using DAVID bioinformatics resources. Nat Protoc 2009;4(1):44-57. doi: 10.1038/nprot.2008.211. Huang Da W, Sherman BT, Lempicki RA. Bioinformatics enrichment tools: paths toward the comprehensive functional analysis of large gene lists. Nucleic Acids Res 2009;37(1):1-13. doi: 10.1093/nar/gkn923)* using differentially expressed genes and genes with differentially spliced events.

In vitro studies

1) Effects of anti-citrullinated protein antibodies on HD-leukocytes subsets

IgGs from serum of 5 RA patients with high titers of anti–citrullinated protein antibodies (ACPAs) and negative for RF were isolated using HiTrap protein-G-HP columns (GE Healthcare, Chicago, IL, USA). IgG-ACPAS were subsequently purified using CCP affinity columns as previously described (Barbarroja N et al., ATVB 2014). Briefly, Streptavidin agarose columns (Thermo Fisher Scientific, Waltham, MA, USA) were coupled with biotinylated CCP peptides

following the manufacturer's recommendations (EZ-Link Sulfo-NHS-LC-LC-Biotin, Thermo Fisher Scientific). A cyclic-CCP peptide was synthesized according to the sequence previously designed by Schellekens et al (Arthritis Rheum 2000; 43:155–63) for the clinical test of ACPAS (Immunostep, Salamanca, Spain): HQCHQESTXGRSRGRCGRSGS, where X refers to citrulline. The IgGs-containing ACPAs from RA serum were incubated with the CCP affinity column 6 hours at room temperature. Afterward, the column was washed with PBS to obtain the flow through with IgGs depleted in ACPAS. Finally, IgG-ACPAS were eluted with 0.1M Glycine-hydrogen chloride (HCL) pH2.5 and neutralized with 2M Tris. The activity of both, IgG-ACPA and flow-through (IgGs depleted in ACPAS) was confirmed by ELISA (Immunoscan CCPlus, SVAr Life Science, Sweden).

Then, 500,000 cells/well from HD peripheral blood leukocytes subsets were treated with purified IgG-ACPAS and flow-through (IgG depleted in ACPAS) (10 ug/ml), either for 6 h (neutrophils) or for 24 h (monocytes and lymphocytes), and effects on SM components and inflammatory cytokines were assessed.

To evaluate the effects of FcR (Fc receptor) blockage, monocytes, lymphocytes and neutrophils were preincubated with FcR Blocking Reagent (Miltenty) for 15 minutes at 4 °C before the treatment with purified IgG-ACPAS and flow-through (IgG depleted in ACPAS), as above described.

To further validate the specificity of ACPAS, parallel experiments were carried out using human monoclonal ACPAS (anticitrullinated fibrinogen immunoglobulin, clone 1F11,10 µg/ml) (MQR 2.101-100, Modiquest, Molenweg, The Netherlands) and synthetic human IgG (Jackson InmunoResearch Laboratories, Inc, Newmarket, Suffolk, UK).

Lastly,

2) <u>Effects of inflammatory cytokines on the expression of SME in HD leukocytes subsets</u>

500,000 cells/well from HD peripheral blood leukocytes subsets were treated with purified TNFa, IL6, and CCL2 (20 ng/ml each) either for 6 h (neutrophils) or for 24 h (monocytes and lymphocytes), and effects on SM components were assessed by RT-PCR.

3) <u>Transfection studies</u>

Peripheral blood leukocytes subsets from 4 RA patients were used for *transfection* studies. Briefly, 500,000 cells/well were transiently overexpressed using Lipofectamine 2000 (Life Technologies) with *KHDRBS1* (OHu20035, Genscript, Leiden, The Netherlands) or *SNRNP70* (OHu21864, Genscript) vectors for 24h, being the empty pCDNA3.1^{+} (mock, Life Technologies, Grand Island, NY, USA) used as negative control, as previously described.[32]

Then, effectiveness of transfections was assessed by RT-PCR and Western blot assays. A 27-plex panel of secreted inflammatory molecules was assessed in RA-lymphocytes; adhesion was evaluated on RA-monocytes after 24 h using Vybrant cell adhesion kit (Molecular Probes Inc, Leiden, The Netherlands); nucleosomes and neutrophil elastase were assessed in the supernatant of RA-neutrophils using the ELISAPLUS kit for detection of human cell death (Roche Diagnostics) and the Human Elastase PMN Sandwich ELISA Kit (Abcam, Cambridge, UK), respectively.

4) Effects of supernatants from transfected lymphocytes on functional activity of synovial fibroblasts.

For isolation of synovial fibroblasts (SF), synovial fluid was aspirated from joints of 10 patients with established and active RA. Fluid was collected in heparinized syringes, then centrifuged at 1200 rpm for 15 min. The resulting cell pellet was resuspended in 7 ml of growth medium [DMEM / F12 (1:1) HAM with 15% heat inactivated fetal bovine serum (FBS), 2mM l-glutamine, 1% penicillin/streptomycin solution (Sigma)], supplemented with fibroblast growth factor beta (FGFb, 1 ng/ml) and plated in 25 ml tissue culture flasks. Cultures were incubated at 37°C with 5% CO_2 for 24 to 48 h, after which medium was aspirated and cultures were washed with phosphate buffered saline (PBS) to remove nonadherent cells. Growth medium was replaced every 3 to 4 days. After 10 to 14 days, adherent cells were removed from flasks by trypsinization, washed, and transferred to 75 ml tissue culture flasks in fresh growth medium. Purified SF were passaged (split 1:3) when they reached confluence, generally at 10 to 14 days. Passages 2 through 6 were used for experiments.

Cultured SF were grown either in 96-well culture plates (5.000 cells/well) or 24-well culture plates (500.000 cells/well), and subsequently stimulated for 24h with the supernatant obtained from transfection cultures (diluted 1:1 with growth medium).

Then, SF proliferation and migration were measured using resazurin and wound-healing assays, respectively, as previously reported (*Jiménez-Vacas JM, Herrero-Aguayo V, Gómez-Gómez E, et al. Spliceosome component SF3B1 as novel prognostic biomarker and therapeutic target for prostate cancer. Transl Res 2019;212:89-103. doi: 10.1016/j.trsl.2019.07.001*). Gene expression of inflammatory mediators was evaluated by RT-PCR.

Identification of the citrullinome in PBMCs by LC-MS/MS

Sample preparation and LC-MS/MS analysis

Equal amounts of each sample pool (approximately 10µg) were reduced with 10 mM dithiothreitol for 1 h at 37 °C, and subsequently alkylated with 50 mM iodoacetamide for 45 minutes at room temperature in the dark. Samples were digested with sequencing grade modified trypsin (Promega) at 1:40 enzyme-to-substrate ratio. After 16 h of digestion at 37 °C, samples were acidified with 10% trifluoroacetic acid to ~pH 3. The digested peptides were desalted using in-house made stage tips (3M Empore SPE-C18 disk, 47 mm, Sigma Aldrich) and finally dried under speed-vacuum (Thermo, USA). The dried eluates were re-constituted in water with 2% acetonitrile (ACN) and 0.1% FA for direct LC-MS. The peptide mixture (200ng) was loaded in a nanoElute (Bruker Daltonics) nano-flow LC coupled to a high-resolution TIMS-QTOF (timsTOF Pro, Bruker Daltonics) with a CaptiveSpray ion source (Bruker Daltonics). Liquid chromatography was performed at 50 °C and with a constant flow of 500 nL/min on a reversed-phase column (15 cm * 75 m i.d.) with a pulled emitter tip, packed with 1.9 m C18-coated porous silica beads (Dr. Maisch, Ammerbuch-Entringen, Germany). Chromatographic separation was carried out using a linear gradient of 5-35% buffer B (100% ACN and 0.1% FA) over 60 min. After ESI ionization, peptides were analyzed in data-dependent mode with Parallel Accumulation–Serial Fragmentation (PASEF) enabled.

Data analysis

Mass spectrometry raw files were processed with PEAKS Studio 10.6 build 20201221 (Bioinformatics solutions Inc.). The MS/MS spectra were matched to *in silico* derived fragment mass values of tryptic peptides against the UniProtKB/Swiss-Prot human database (release 2021_02). Search parameters were: Parent Mass Error Tolerance: 15.0 ppm; Fragment Mass Error Tolerance: 0.05 Da; Enzyme: Trypsin; Fixed Modifications: Carbamidomethylation; Variable Modifications: Acetylation (Protein N-term), Deamidation (NQ), Oxidation (M), Acetylation (N-term) and Citrullination (R); Max Variable PTM Per Peptide: 3. Matches were filtered for 1% FDR at peptide level.
For PTMs quantification, citrullinated peptides with AScore >20 (p value < 0.01) (PMID: 16964243) were considered.

Quantification of citrullination was calculated as the sum of intensities of all redundant identifications of a peptide in a certain citrullination state, divided by the sum of intensities of all identifications of the same peptide, independently of modifications.

Statistical analysis

Data were expressed as mean ± SEM or median ± IQR according to data distribution, evaluated using Kolmogorov-Smirnov test. Thus, Student's t test or Mann-Whitney rank sum test were used to assess statistical differences in unpaired data, and paired t tests and Wilcoxon matched-pairs signed rank tests for paired data. The chi-square test was used to associate qualitative variables. Correlations were evaluated by Spearman's correlation test. In addition, for adjusting the p-values towards multiple hypothesis testing, a Benjamini Hochberg-based false discovery rate (FDR) was applied (REF). Statistically significant differences were considered at p-value<0.05 and FDR<0.15 (*Y. Benjamini and Y. Hochberg, Controlling the False Discovery Rate-a Practical and Powerful Approach to Multiple Testing, J. Roy. Stat. Soc. B Stat. Methodol., 1995, 57, 289-300).*

Logistic regression models were calculated using the formula $= \frac{1}{1+e^{-(\beta 0+\beta 1x1.i+\cdots+\beta kxk.i)}}$, being β_i the coefficients of the parameters. Receiver operating characteristic (ROC) curves were performed to evaluate the specificity and sensibility of the different diagnostic or discriminating models. Statistical analysis of each ROC curve was performed by evaluating the area under the curve (AUC) of each model and comparing them with the reference line.

Data analyses were performed using SPSS 24.0 (IBM, Chicago, IL, USA) and GraphPad Prism 8.0 (GraphPad Software, La Jolla, CA).

SUPPLEMENTAL FIGURES

Supplemental Figure 1. Spliceosome components are dysregulated in a coordinated way. Heat map of correlation between the signature of 8 spliceosome components commonly altered in neutrophils, monocytes and lymphocytes. Positive and negative correlations are displayed in red or blue respectively accordingly to the Spearman correlation coefficient. Lym, lymphocytes; Mon, monocytes; Neu, neutrophils.

Supplemental Figure 2. RA patients exhibit an altered circulating pro-inflammatory profile. Plasmatic levels of a panel of 27 molecules including cytokines, chemokines and adhesion molecules were analysed by using a multiplex bead-based assay system.

(A) Heat map showing the differential expression of those molecules between RA and HD are shown. Blue and red colours represent downregulated and upregulated pro-inflammatory molecules respectively. (B) Violin plots indicating the expression levels of differentially expressed pro-inflammatory molecules in plasma from RA and HD. *p<0.05, **p<0.01, ***p<0.001. RA, Rheumatoid Arthritis; HD, Healthy Donors.

Supplemental Figure 3. Differential expression of SME in whole blood cells and synovial biopsies. Heatmap showing unsupervised hierarchical clustering of expression-pattern change of splicing machinery and splicing factors. Normalized transcripts have been scaled by autoscaling method to perform the heatmap.

Supplemental Figure 4.- The SME expression pattern is associated with differential splice events, splice variants, and gene pathways. A. Volcano-plots where the ΔΨ of total events calculated is plotted against the –log10 (p-value) of the Fisher's Exact Test to assay differentially expressed splicing variants between high and low SME expression groups of samples. B. Relative frequency of each alternative splicing event between low and high SME expression groups. C. UpSet plot for all transcript variants generated. Strips show the number of differentially spliced transcripts significantly different between low and high SME expression. Dots and lines represent specific transcripts. The histogram represents the number of differentially spliced transcripts.

Supplemental Figure 5.- Enrichment plots according to differential splicing variants. Gene Ontology (GO) terms enrichment analyses were performed using DAVID online software, using genes with differentially spliced events.

Supplemental Figure 6.- Enrichment plots according to differential expressed genes. A. Gene Ontology (GO) terms enrichment analyses were performed using DAVID online software, using differentially expressed genes. **B**. Volcano-plots where the $\log_2$ (Fold Change) of total differentially expressed genes is plotted against the $-\log_{10}$ (p-value) of the Fisher's Exact Test to assay differentially expressed genes between high and low SME expression groups of samples.

Supplemental Figure 7. Anti-TNF therapy for six months reverse the altered spliceosome signature of whole blood along with the inflammatory and clinical profile in RA patients. (A) Table showing clinical and serological characteristics of 25 responders RA patients before and after 6 months of TNFi therapy. (B) Heat map showing levels of circulating inflammatory molecules in plasma of RA patients before and after 6 months of TNFi therapy. Levels of inflammatory molecules are expressed as log 2 and normalized to time 0 (T0), before therapy in responders RA patients. (C) Violin plots representing the expression distribution of the 8 spliceosome components in whole blood before and after 6 months of TNFi therapy in responders' RA patients. *p < 0.05, **p < 0.01. T0, time before TNFi therapy; T6, time 6 months after TNFi therapy; R, responders RA patients.

Supplemental Figure 8. In vitro treatment of healthy leukocytes in the presence of FcR blockers prevents the alterations of SME induced by ACPAs. Monocytes (A, D), lymphocytes (B, E) and neutrophils (C, F) from healthy donors were preincubated with

FcR Blocking Reagent (Miltenty) for 15 minutes at 4 °C before the treatment with 10 ug/ml of either, IgG-ACPA purified from RA patients through CCP-affinity column chromatography [IgG-ACPAS (+)] or the flow through depleted in Ig-ACPAS [IgG-ACPAS(-)] for 24 in monocytes and lymphocytes and 6 h in neutrophils. Spliceosome components (A, B, C) and inflammatory molecules (D, E, F) were analysed by RT-PCR. Data from 5 independent experiments carried out in triplicate are shown. *p < 0.05, **p < 0.01, IgG, immunoglobulin G; ACPAs, Anti-citrullinated protein antibodies.

Supplemental Figure 9. In vitro treatment of healthy leukocytes with monoclonal ACPAs modify the expression of the spliceosome signature along with their associated inflammatory profile. Monocytes (A, D), lymphocytes (B, E) and neutrophils (C, F) from healthy donors were treated with 10 ug/ml of a monoclonal IgG-ACPA (human monoclonal anticitrullinated fibrinogen immunoglobulin, clone 1F11) and a commercial IgG control (human IgG Jackson InmunoResearch Laboratories, Inc, Newmarket, Suffolk, UK) for 24 in monocytes and lymphocytes and 6 h in neutrophils. Spliceosome components (A, B, C) and inflammatory molecules (D, E, F) were analysed by RT-PCR. Data from 5 independent experiments carried out in triplicate are shown. *p < 0.05, **p < 0.01, IgG, immunoglobulin G; ACPAs, Anti-citrullinated protein antibodies.

Supplemental Figure 10. Citrullination status of PBMCs from RA patients associated to the SME alteration. A) Diagram showing the experimental design. RA patients were selected based on their opposite patterns of SME alteration analyzed previously by RT-PCR. Cell lysates from PBMC of 10 RA patients belonging to the first (5 patients) and third tercile (5 patients) mainly characterized by high ("mild SME alteration") and low ("severe SME alteration") levels of SME respectively were pooled and the global citrullination status was assessed by Liquid Chromatography with tandem mass spectrometry (LC-MC/MS). B) Levels of the 8 SME in PBMC from RA patients selected by using RT-PCR. C) Quantification of the global citrullination status in each pooled sample from PBMCs of RA patients. Mass spectrometry raw files were processed with PEAKS Studio 10.6 and total label-free quantification intensities (LFQ) were obtained. D) Citrullination status of well-stablished proteins as autoantigens of ACPAS in PBMCs from RA patients with differential SME alteration status. *p<0.05

Supplemental Figure 11. Effect of Cytokines in the expression of splicing machinery elements (SME) from healthy leukocytes. Three cytokines with a key role in the pathogenesis of RA were added to monocytes, lymphocytes and neutrophils (10 ng/ml) purified from healthy donors. After 6 hours of treatment in neutrophils and 24 hours in monocytes and lymphocytes, SME levels were analyzed by RT-PCR. Data from 5 independent experiments carried out in triplicate are shown. *p<0.05

Supplemental Figure 12. Impact of the modulation of the lymphocyte-splicing machinery elements in synovial fibroblast phenotype. A) Schematic representation of the experimental design. Supernatant from RA lymphocyte transfected with mock, KHDRBS1 and SNRNP70 were added to synovial fibroblast (SF) and its impact was

Ibáñez-Costa A, *et al. Ann Rheum Dis* 2021; 81:56–67. doi: 10.1136/annrheumdis-2021-220308

evaluated through functional assays after 24 hours of culture. B) Migration capacity of SF was evaluated through wound-healing assay. C) Proliferation rate of SF was studied by using resazurin-based fluorescent dye based assay. D) Activation status of SF was analyzed through RT-PCR where genes related to cytokine and chemokine activity and collagen fibrin organization were assessed. Data from 5 independent experiments carried out in triplicate are shown. Data from 4 independent experiments carried out in triplicate are shown. * $p<0.05$

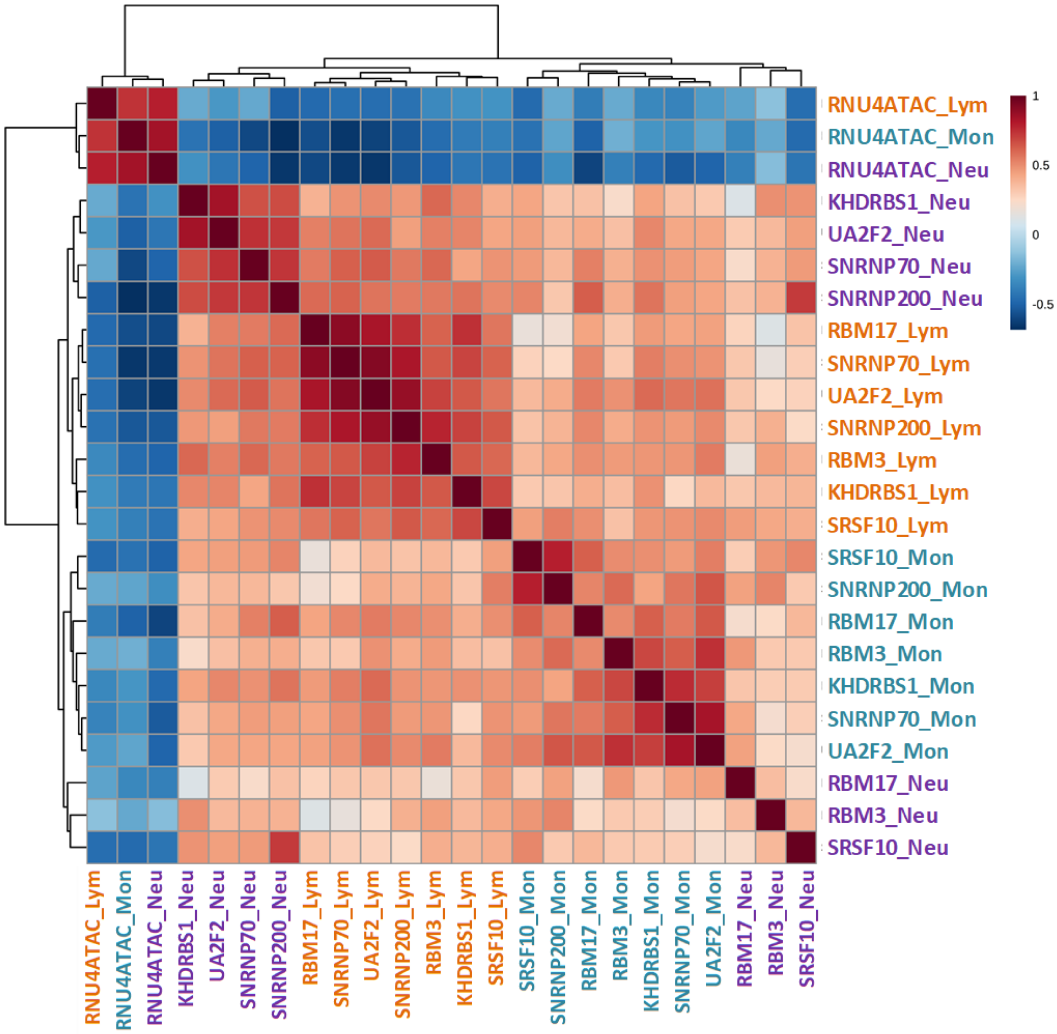

Supplemental Figure 1

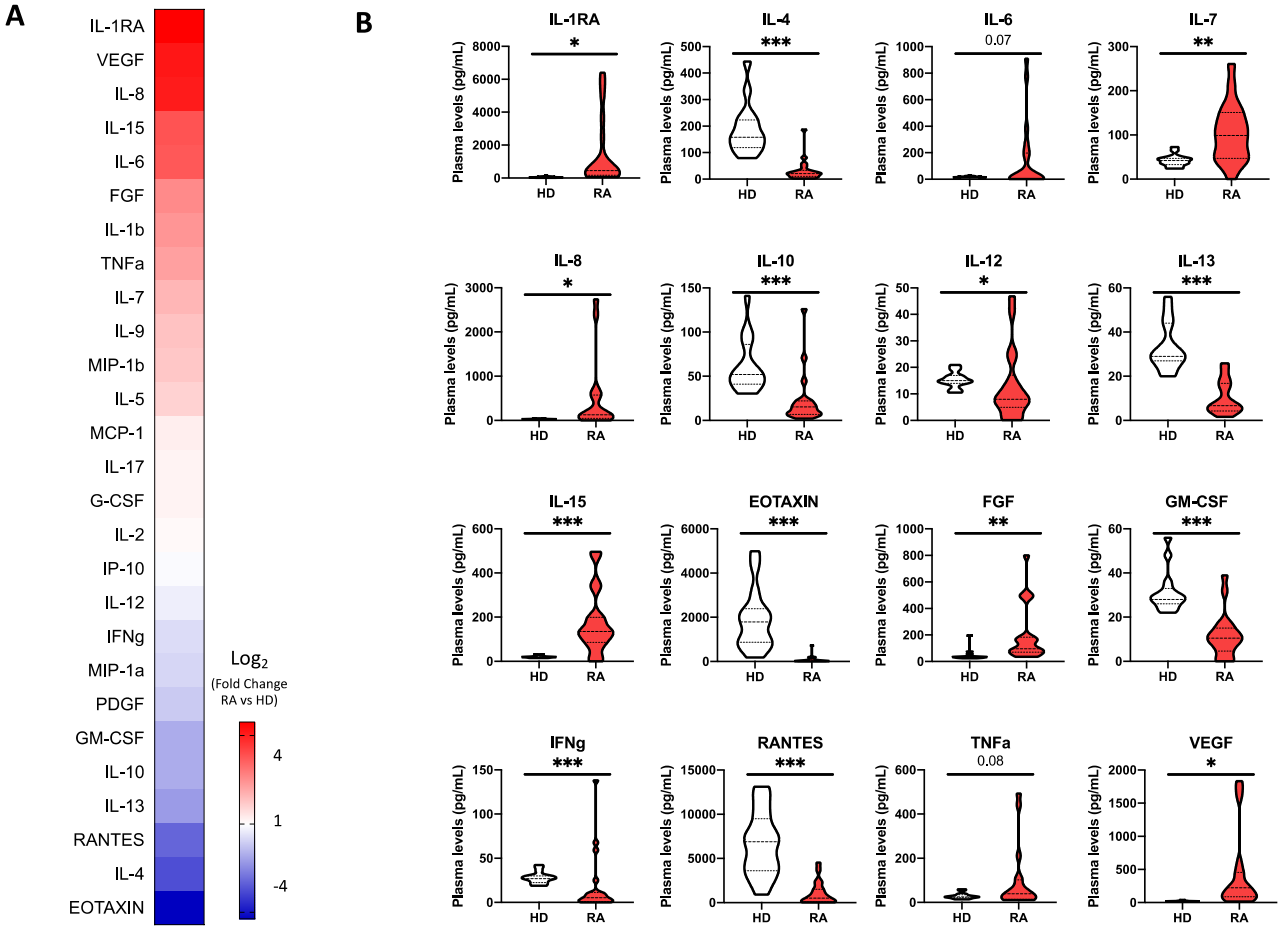

Supplemental Figure 2

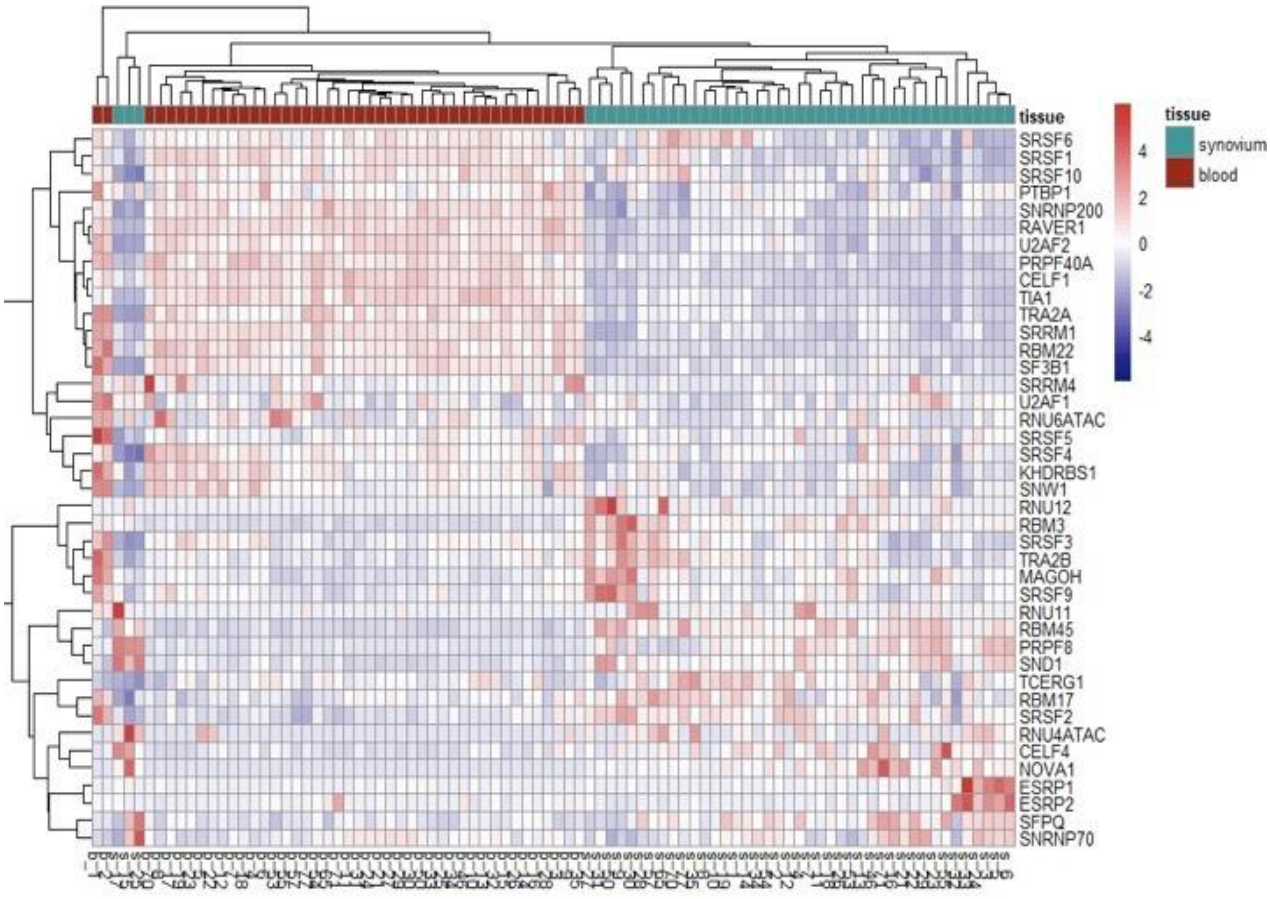

Supplemental Figure 3

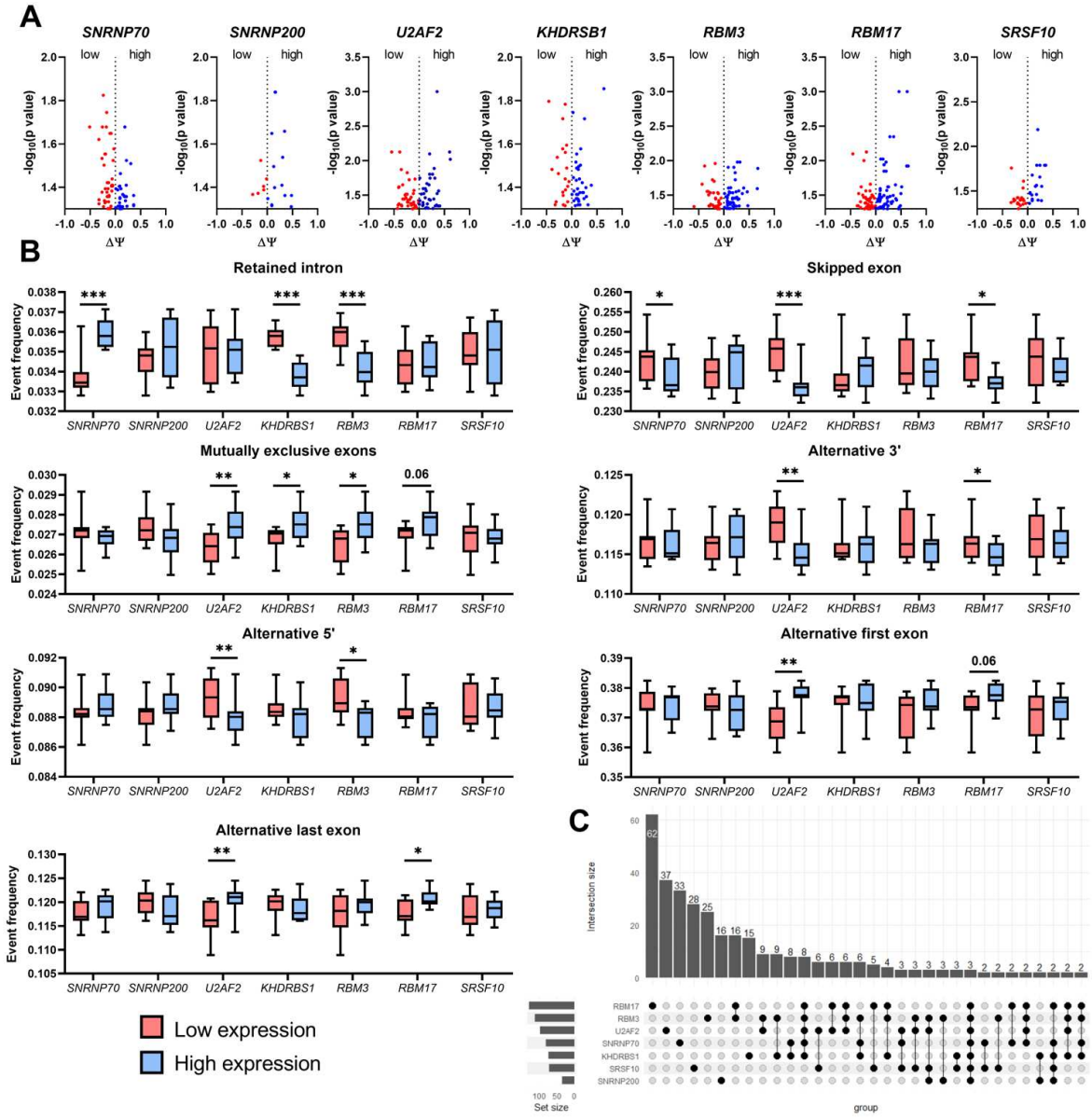

Supplemental Figure 4

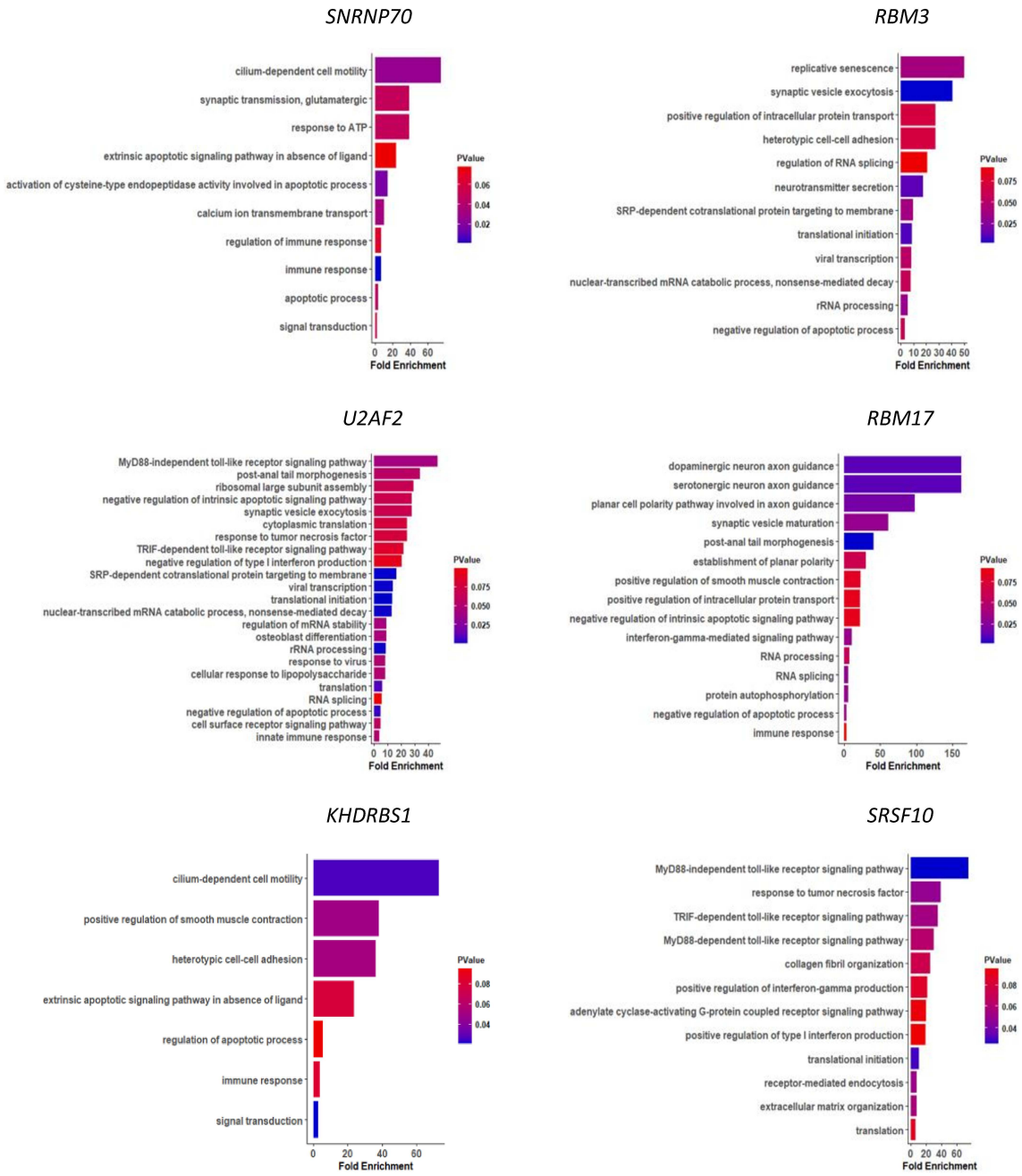

Supplemental Figure 5

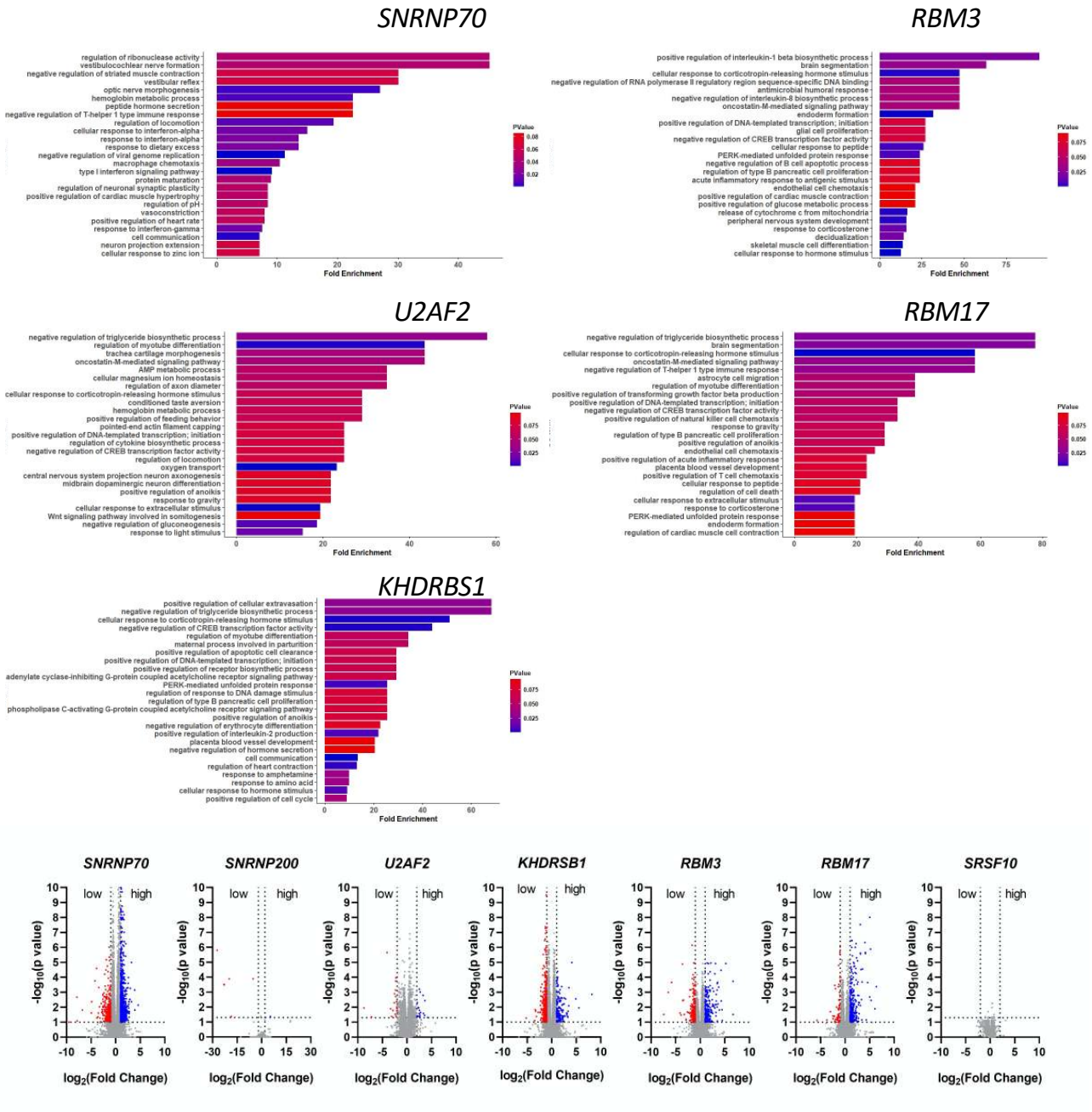

Supplemental Figure 6

A

	Responders (n=25)		
	Before TNFi	After TNFi	p
Clinical parameters			
Female/male, n/n	21/4	-	
Age, y	53 ± 11	-	
Evolution time, y	10 ± 8	-	
Swollen joints (n)	4,7 ± 3,9	0,8 ± 1,1	**0,001**
Tender joints (n)	8,9 ± 6,4	2,9 ± 6,6	**<0,001**
DAS28	4,8 ± 1,1	2,9 ± 1,3	**<0,001**
VAS	60,9 ± 27,0	32,1 ± 26,4	**<0,001**
HAQ	1,4 ± 0,8	1,3 ± 0,7	0,069
Serological assessments			
Anti-CCP levels (U/mL)	296,4 ± 281,2	166,6 ± 158,9	0,216
Rheumatoid Factor levels (IU/mL)	65,4 ± 77,6	74,8 ± 92,8	0,397
CRP, mg/dL	10,3 ± 8,2	5,7 ± 7,8	**0,009**
ESR, mm/h	29,9 ± 15,9	26,9 ± 18,6	0,384

B

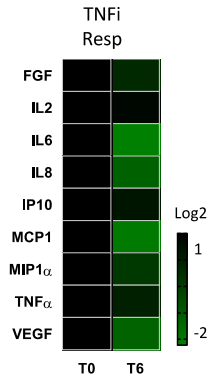

C

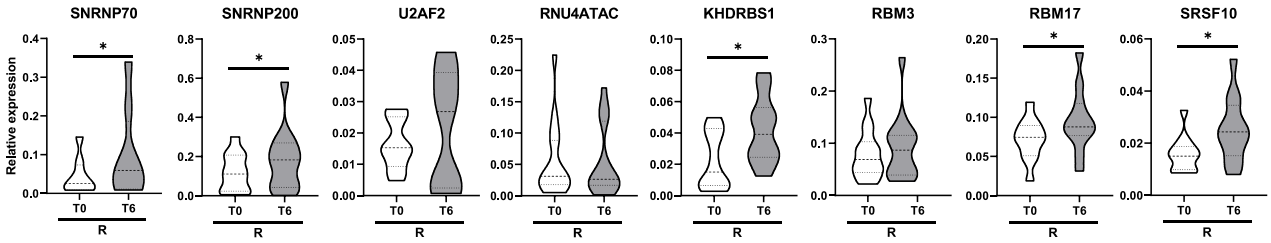

Supplemental Figure 7

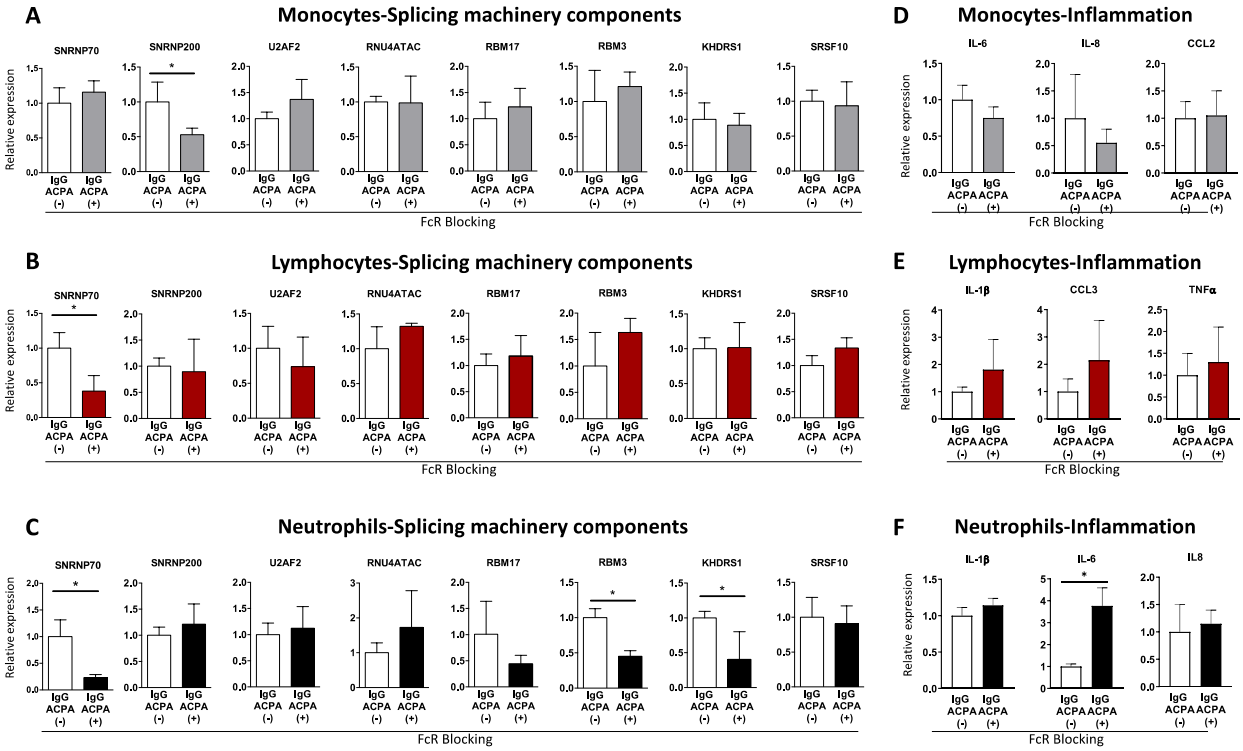

Supplemental Figure 8

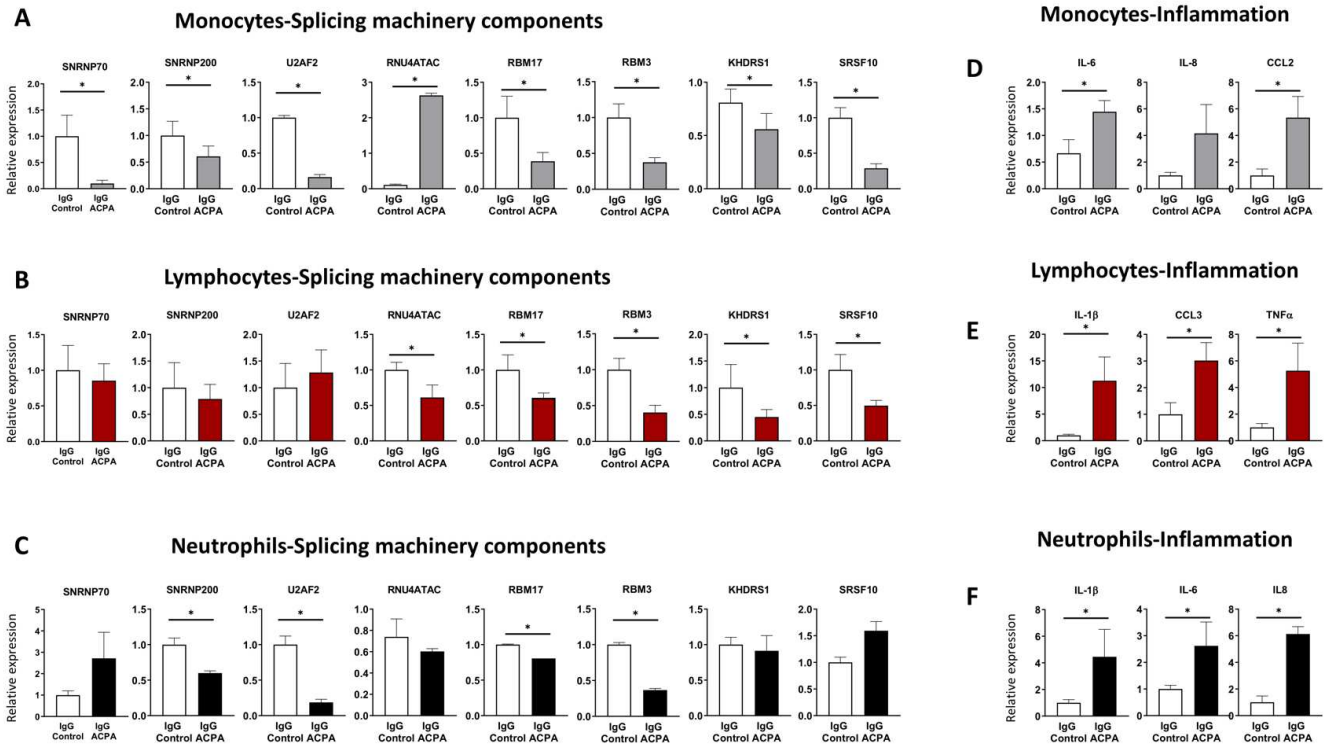

Supplemental Figure 9

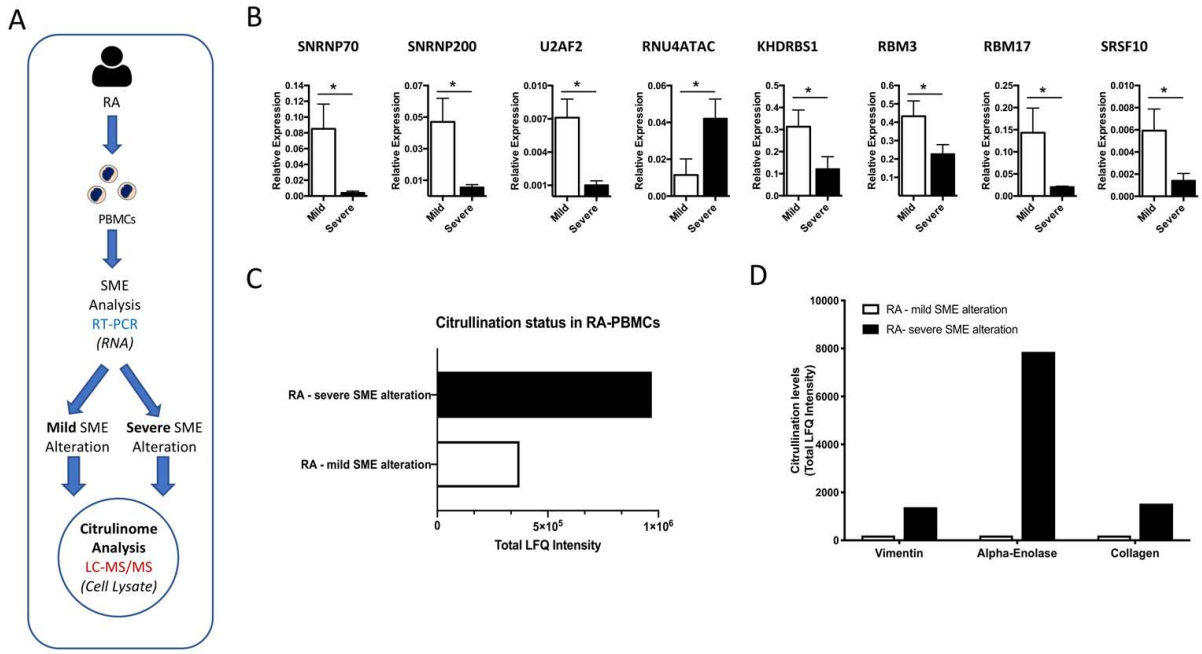

Supplemental Figure 10

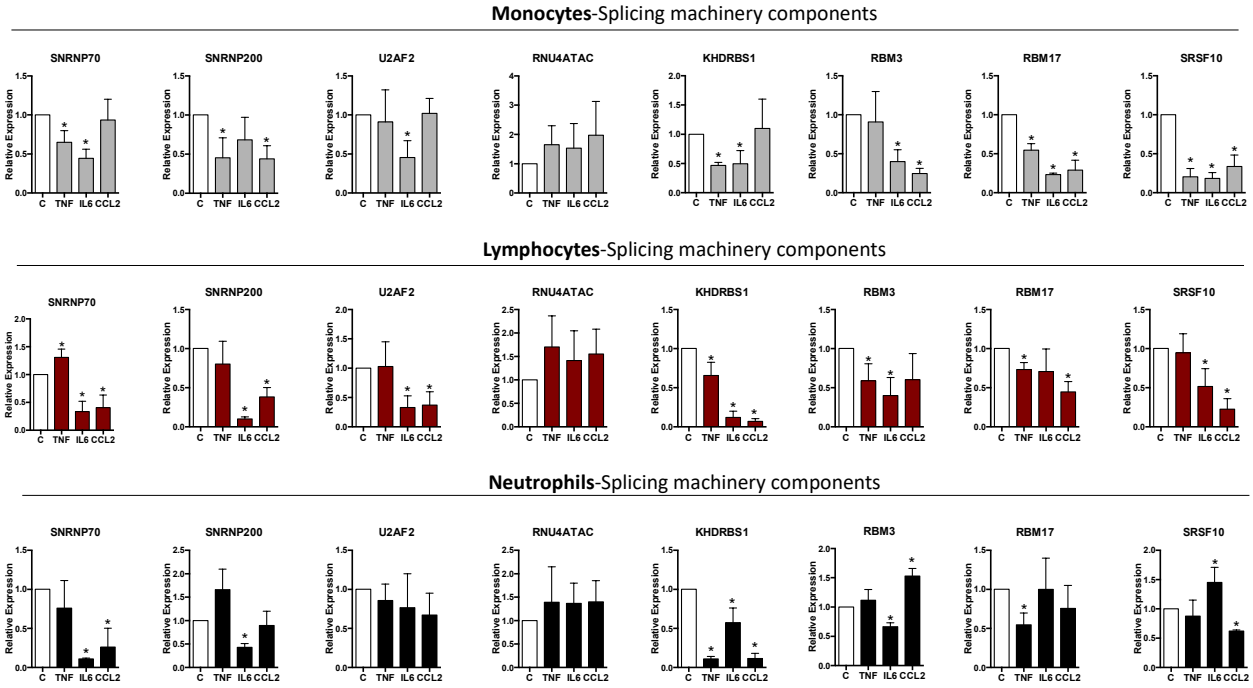

Supplemental Figure 11

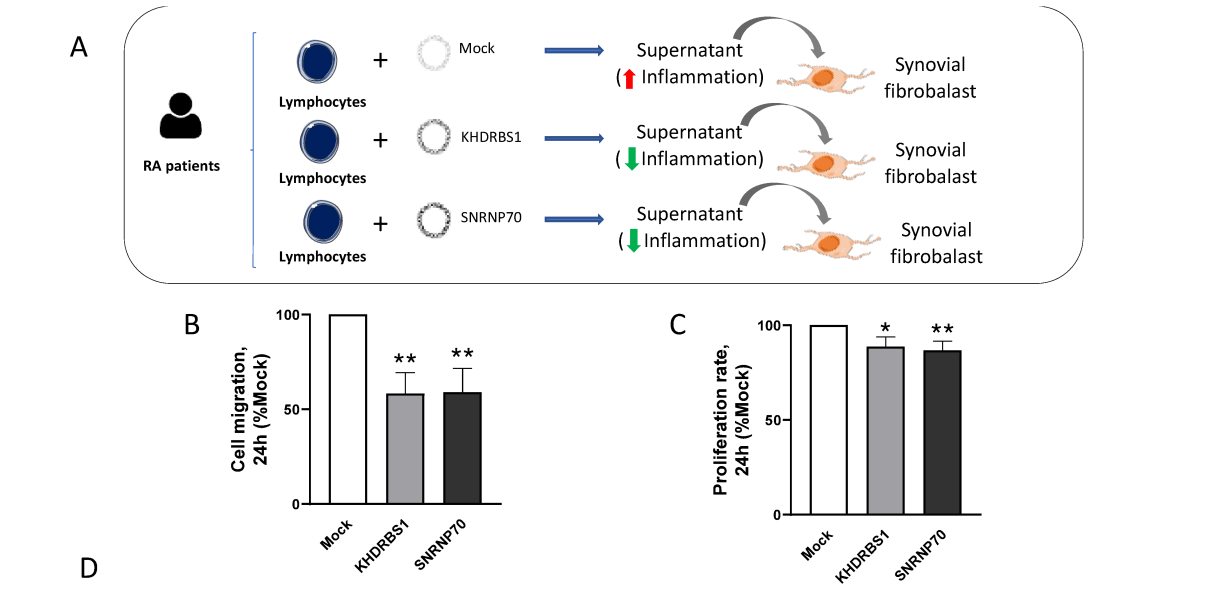

Supplemental Figure 12

SUPPLEMENTAL TABLES

Supplemental Table 1. List of primer sequences for inflammatory and selected splicing machinery components mRNAs

GENE	***SEQUENCE***	
	Forward	***Reverse***
GAPDH	TGTAGTTGAGGTCAATGAAGGG	ACATCGCTAGACACCATG
IL1B	CAGATTCTTTTCCTTGAGGC	GCAACAAGTGGTGTTCTC
IL2	CACTAAGTCTTGCACTTGTC	CTTAAATGTGAGCATCCTGG
IL6	AAGATTCCAAAGATGTAGCC	ACATGTCTCCTTTCTCAGG
IL8	TACTCCAAACCTTTCCACC	CTCAGCCCTCTTCAAAAAC
IL12A	ATGAGAGTTGCCTAAATTCC	CATAAAAGAGGTCTTTCTGGAG
IL17A	GTATGAGAAAAGTTCAGCCC	TGGTTACGATGTGAAACTTG
IFNG	GGTAACTGACTTGAATGTCC	TTTTCGCTTCCCTGTTAG
IP10	AAAGCAGTTAGCAAGGAAAG	TCATTGGTCACCTTTTAGTG
MCP1	CTATAGAAGAATCACCAGCAG	CTAGGGGAAAATAAGTTAGCTG
RANTES	ATCTGCCTCCCCATATTC	AAGAGTTGATGTACTCCCG
TF	GTGAAGAAATCAGCTTCTGAC	ATTCATCAAATCTGCAGTGG
TNF	CTCAGCCTCTTCTCCTTC	AGAAGATGATCTGACTGCC
VEGFA	GACCAAAGAAAGATAGAGCAAG	ATACGCTCCAGGACTTATAC
SNRNP70	TCTTCGTGGCGAGAGTGAAT	GCTTTCCTGACCGCTTACTG
SNRNP200	GGTGCTGTCCCTTGTTGG	CTTTCTTCGCTTGGCTCTTCT
U2AF2	CTTTGACCAGAGGCGCTAAA	TACTGCATTGGGGTGATGTG
RNU4ATAC	GTTGCGCTACTGTCCAATGA	CAAAAATTGCACCAAAATAA
RBM17	CAAAGAGCCAAAGGACGAAA	TACATGCGGTGGAGTGTCC
RBM3	AAGCTCTTCGTGGGAGGG	TTGACAACGACCACCTCAGA
KHDRBS1	GAGCGAGTGCTGATACCTGTC	CACCAGTCTCTTCCTGCAGTC
SRSF10	CTACACTCGCCGTCCAAGAG	CCGTCCACAAATCCACTTTC

Supplemental Table 2. Citrullinated proteins in PBMCs from Rheumatoid Arthritis patients identified by mass spectrometry

Citrullinated Protein	Protein Description	Protein Position	Modified Peptide Sequence
Q9Y490|TLN1_HUMAN	Talin-1 OS=Homo sapiens OX=9606 GN=TLN1 PE=1 SV=3	R181	LNWLDHGRTLrEQGVEEHETL
	Talin-1 OS=Homo sapiens OX=9606 GN=TLN1 PE=1 SV=3	R207	FFYSDQNVDSrDPVQLNLLYV
	Talin-1 OS=Homo sapiens OX=9606 GN=TLN1 PE=1 SV=3	R454	HGSVALPAIMrSGASGPENFQ
	Talin-1 OS=Homo sapiens OX=9606 GN=TLN1 PE=1 SV=3	R1222	ALRAVGDASKrLLSDSLPPST
	Talin-1 OS=Homo sapiens OX=9606 GN=TLN1 PE=1 SV=3	R1241	STGTFQEAQSrLNEAAAGLNQ
	Talin-1 OS=Homo sapiens OX=9606 GN=TLN1 PE=1 SV=3	R1523	SARTTNPTAKrQFVQSAKEVA
	Talin-1 OS=Homo sapiens OX=9606 GN=TLN1 PE=1 SV=3	R1618	ESAGGLIQTArALAVNPRDPP
	Talin-1 OS=Homo sapiens OX=9606 GN=TLN1 PE=1 SV=3	R2197	AKAVAAGNSCrQEDVIATANL
	Talin-1 OS=Homo sapiens OX=9606 GN=TLN1 PE=1 SV=3	R2210	DVIATANLSRrAIADMLRACK
	Talin-1 OS=Homo sapiens OX=9606 GN=TLN1 PE=1 SV=3	R2368	ALVKAASAAQrELVAQGKVGA
	Talin-1 OS=Homo sapiens OX=9606 GN=TLN1 PE=1 SV=3	R2538	QQYKFLPSELrDEH*******
P21333|FLNA_HUMAN	Filamin-A OS=Homo sapiens OX=9606 GN=FLNA PE=1 SV=4	R7	****MSSSHSrAGQSAAGAAP
	Filamin-A OS=Homo sapiens OX=9606 GN=FLNA PE=1 SV=4	R24	GAAPGGGVDTrDAEMPATEKD
	Filamin-A OS=Homo sapiens OX=9606 GN=FLNA PE=1 SV=4	R301	IEPTGNMVKKrAEFTVETRSA
	Filamin-A OS=Homo sapiens OX=9606 GN=FLNA PE=1 SV=4	R678	QDFHPDRVKArGPGLEKTGVA
	Filamin-A OS=Homo sapiens OX=9606 GN=FLNA PE=1 SV=4	R828	AEADIDFDIIrNDNDTFTVKY
	Filamin-A OS=Homo sapiens OX=9606 GN=FLNA PE=1 SV=4	R1032	PGLGADNSVVrFLPREEGPYE
	Filamin-A OS=Homo sapiens OX=9606 GN=FLNA PE=1 SV=4	R2003	REEPCLLKRLrNGHVGISFVP
	Filamin-A OS=Homo sapiens OX=9606 GN=FLNA PE=1 SV=4	R2288	PSKAEISFEDrKDGSCGVAYV
	Filamin-A OS=Homo sapiens OX=9606 GN=FLNA PE=1 SV=4	R2391	TEIDQDKYAVrFIPRENGVYL
	Filamin-A OS=Homo sapiens OX=9606 GN=FLNA PE=1 SV=4	R2395	QDKYAVRFIPrENGVYLIDVK

Ibáñez-Costa A, *et al. Ann Rheum Dis* 2021; 81:56–67. doi: 10.1136/annrheumdis-2021-220308

	Filamin-A OS=Homo sapiens OX=9606 GN=FLNA PE=1 SV=4	R2484	MDCQECPEGYrVTYTPMAPGS
P60709|ACTB_HUMAN	Actin cytoplasmic 1 OS=Homo sapiens OX=9606 GN=ACTB PE=1 SV=1	R62	SYVGDEAQSKrGILTLKYPIE
	Actin cytoplasmic 1 OS=Homo sapiens OX=9606 GN=ACTB PE=1 SV=1	R177	EGYALPHAILrLDLAGRDLTD
	Actin cytoplasmic 1 OS=Homo sapiens OX=9606 GN=ACTB PE=1 SV=1	R312	GTTMYPGIADrMQKEITALAP
	Actin cytoplasmic 2 OS=Homo sapiens OX=9606 GN=ACTG1 PE=1 SV=1	R62	SYVGDEAQSKrGILTLKYPIE
	Actin cytoplasmic 2 OS=Homo sapiens OX=9606 GN=ACTG1 PE=1 SV=1	R177	EGYALPHAILrLDLAGRDLTD
	Actin cytoplasmic 2 OS=Homo sapiens OX=9606 GN=ACTG1 PE=1 SV=1	R312	GTTMYPGIADrMQKEITALAP
P35579|MYH9_HUMAN	Myosin-9 OS=Homo sapiens OX=9606 GN=MYH9 PE=1 SV=4	R159	HIYAITDTAYrSMMQDREDQS
	Myosin-9 OS=Homo sapiens OX=9606 GN=MYH9 PE=1 SV=4	R1923	EVSSLKNKLRrGDLPFVVPRR
P68032|ACTC_HUMAN	Actin alpha cardiac muscle 1 OS=Homo sapiens OX=9606 GN=ACTC1 PE=1 SV=1	R64	SYVGDEAQSKrGILTLKYPIE
P18206|VINC_HUMAN	Vinculin OS=Homo sapiens OX=9606 GN=VCL PE=1 SV=4	R502	HLEGKIEQAQrWIDNPTVDDR
	Vinculin OS=Homo sapiens OX=9606 GN=VCL PE=1 SV=4	R538	RLANVMMGPYrQDLLAKCDRV
P07996|TSP1_HUMAN	Thrombospondin-1 OS=Homo sapiens OX=9606 GN=THBS1 PE=1 SV=2	R20	LFLMHVCGTNrIPESGGDNSV
	Thrombospondin-1 OS=Homo sapiens OX=9606 GN=THBS1 PE=1 SV=2	R479	MNGKPCEGEArETKACKKDAC
P14618|KPYM_HUMAN	Pyruvate kinase PKM OS=Homo sapiens OX=9606 GN=PKM PE=1 SV=4	R279	SKIENHEGVRrFDEILEASDG
	Pyruvate kinase PKM OS=Homo sapiens OX=9606 GN=PKM PE=1 SV=4	R294	LEASDGIMVArGDLGIEIPAE
	Pyruvate kinase PKM OS=Homo sapiens OX=9606 GN=PKM PE=1 SV=4	R376	AKGDYPLEAVrMQHLIAREAE
P08670|VIME_HUMAN	Vimentin OS=Homo sapiens OX=9606 GN=VIM PE=1 SV=4	R196	REKLQEEMLQrEEAENTLQSF
	Vimentin OS=Homo sapiens OX=9606 GN=VIM PE=1 SV=4	R273	PDLTAALRDVrQQYESVAAKN
	Vimentin OS=Homo sapiens OX=9606 GN=VIM PE=1 SV=4	R304	KFADLSEAANrNNDALRQAKQ
	Vimentin OS=Homo sapiens OX=9606 GN=VIM PE=1 SV=4	R381	NMKEEMARHLrEYQDLLNVKM
	Vimentin OS=Homo sapiens OX=9606 GN=VIM PE=1 SV=4	R410	YRKLLEGEESrISLPLPNFSS
P05106|ITB3_HUMAN	Integrin beta-3 OS=Homo sapiens OX=9606 GN=ITGB3 PE=1 SV=2	R93	PVSEARVLEDrPLSDKGSGDS
P02788|TRFL_HUMAN	Lactotransferrin OS=Homo sapiens OX=9606 GN=LTF PE=1 SV=6	R462	EGYLAVAVVRrSDTSLTWNSV
P06733|ENOA_HUMAN	Alpha-enolase OS=Homo sapiens OX=9606 GN=ENO1 PE=1 SV=2	R429	SKAKFAGRNFrNPLAK*****

P12814|ACTN1_HUMAN	Alpha-actinin-1 OS=Homo sapiens OX=9606 GN=ACTN1 PE=1 SV=2	R232	LDAEDIVGTArPDEKAIMTYV
	Alpha-actinin-1 OS=Homo sapiens OX=9606 GN=ACTN1 PE=1 SV=2	R350	TLQTKLRLSNrPAFMPSEGRM
	Alpha-actinin-1 OS=Homo sapiens OX=9606 GN=ACTN1 PE=1 SV=2	R614	WDHVRQLVPRrDQALTEEHAR
P07437|TBB5_HUMAN	Tubulin beta chain OS=Homo sapiens OX=9606 GN=TUBB PE=1 SV=2	R2	*********MrEIVHIQAGQC
	Tubulin beta chain OS=Homo sapiens OX=9606 GN=TUBB PE=1 SV=2	R121	ELVDSVLDVVrKEAESCDCLQ
P68371|TBB4B_HUMAN	Tubulin beta-4B chain OS=Homo sapiens OX=9606 GN=TUBB4B PE=1 SV=1	R2	*********MrEIVHLQAGQC
	Tubulin beta-4B chain OS=Homo sapiens OX=9606 GN=TUBB4B PE=1 SV=1	R77	DLEPGTMDSVrSGPFGQIFRP
	Tubulin beta-4B chain OS=Homo sapiens OX=9606 GN=TUBB4B PE=1 SV=1	R121	ELVDSVLDVVrKEAESCDCLQ
P02768|ALBU_HUMAN	Albumin OS=Homo sapiens OX=9606 GN=ALB PE=1 SV=2	R281	HGDLLECADDrADLAKYICEN
Q6S8J3|POTEE_HUMAN	POTE ankyrin domain family member E OS=Homo sapiens OX=9606 GN=POTEE PE=2 SV=3	R762	SYVGKEAQSKrGILTLKYPME
O75083|WDR1_HUMAN	WD repeat-containing protein 1 OS=Homo sapiens OX=9606 GN=WDR1 PE=1 SV=4	R470	VAIGGVDGNVrLYSILGTTLK
P00558|PGK1_HUMAN	Phosphoglycerate kinase 1 OS=Homo sapiens OX=9606 GN=PGK1 PE=1 SV=3	R66	KSVVLMSHLGrPDGVPMPDKY
P06396|GELS_HUMAN	Gelsolin OS=Homo sapiens OX=9606 GN=GSN PE=1 SV=1	R623	AEKTGAQELLrVLRAQPVQVA
	Gelsolin OS=Homo sapiens OX=9606 GN=GSN PE=1 SV=1	R741	IETDPANRDRrTPITVVKQGF
P04075|ALDOA_HUMAN	Fructose-bisphosphate aldolase A OS=Homo sapiens OX=9606 GN=ALDOA PE=1 SV=2	R201	ILPDGDHDLKrCQYVTEKVLA
P11021|BIP_HUMAN	Endoplasmic reticulum chaperone BiP OS=Homo sapiens OX=9606 GN=HSPA5 PE=1 SV=2	R49	YSCVGVFKNGrVEIIANDQGN
	Endoplasmic reticulum chaperone BiP OS=Homo sapiens OX=9606 GN=HSPA5 PE=1 SV=2	R60	VEIIANDQGNrITPSYVAFTP

	Endoplasmic reticulum chaperone BiP OS=Homo sapiens OX=9606 GN=HSPA5 PE=1 SV=2	R74	SYVAFTPEGErLIGDAAKNQL
	Endoplasmic reticulum chaperone BiP OS=Homo sapiens OX=9606 GN=HSPA5 PE=1 SV=2	R492	FDLTGIPPAPrGVPQIEVTFE
P68871|HBB_HUMAN	Hemoglobin subunit beta OS=Homo sapiens OX=9606 GN=HBB PE=1 SV=2	R31	VDEVGGEALGrLLVVYPWTQR
P26038|MOES_HUMAN	Moesin OS=Homo sapiens OX=9606 GN=MSN PE=1 SV=3	R295	MGNHELYMRRrKPDTIEVQQM
P00488|F13A_HUMAN	Coagulation factor XIII A chain OS=Homo sapiens OX=9606 GN=F13A1 PE=1 SV=4	R716	LIASMSSDSLrHVYGELDVQI
P05164|PERM_HUMAN	Myeloperoxidase OS=Homo sapiens OX=9606 GN=MPO PE=1 SV=1	R184	RTITGMCNNRrSPTLGASNRA
	Myeloperoxidase OS=Homo sapiens OX=9606 GN=MPO PE=1 SV=1	R236	LARAVSNEIVrFPTDQLTPDQ
	Myeloperoxidase OS=Homo sapiens OX=9606 GN=MPO PE=1 SV=1	R670	LLACIIGTQFrKLRDGDRFWW
	Myeloperoxidase OS=Homo sapiens OX=9606 GN=MPO PE=1 SV=1	R725	NNIFMSNSYPrDFVNCSTLPA
P20700|LMNB1_HUMAN	Lamin-B1 OS=Homo sapiens OX=9606 GN=LMNB1 PE=1 SV=2	R14	ATPVPPRMGSrAGGPTTPLSP
Q01518|CAP1_HUMAN	Adenylyl cyclase-associated protein 1 OS=Homo sapiens OX=9606 GN=CAP1 PE=1 SV=5	R17	LVERLERAVGrLEAVSHTSDM
Q9BVA1|TBB2B_HUMAN	Tubulin beta-2B chain OS=Homo sapiens OX=9606 GN=TUBB2B PE=1 SV=1	R2	*********MrEIVHIQAGQC
	Tubulin beta-2B chain OS=Homo sapiens OX=9606 GN=TUBB2B PE=1 SV=1	R121	ELVDSVLDVVrKESESCDCLQ
P02675|FIBB_HUMAN	Fibrinogen beta chain OS=Homo sapiens OX=9606 GN=FGB PE=1 SV=2	R285	ENGGWTVIQNrQDGSVDFGRK
Q86UX7|URP2_HUMAN	Fermitin family homolog 3 OS=Homo sapiens OX=9606 GN=FERMT3 PE=1 SV=1	R35	EDPEAESVTLrVTGESHIGGV
	Fermitin family homolog 3 OS=Homo sapiens OX=9606 GN=FERMT3 PE=1 SV=1	R215	PDPLLLQRLPrPSSLSDKTQL
P10809|CH60_HUMAN	60 kDa heat shock protein mitochondrial OS=Homo sapiens OX=9606 GN=HSPD1 PE=1 SV=2	R446	IVLGGGCALLrCIPALDSLTP

P62937|PPIA_HUMAN	Peptidyl-prolyl cis-trans isomerase A OS=Homo sapiens OX=9606 GN=PPIA PE=1 SV=2	R37	DKVPKTAENFrALSTGEKGFG
P06576|ATPB_HUMAN	ATP synthase subunit beta mitochondrial OS=Homo sapiens OX=9606 GN=ATP5F1B PE=1 SV=3	R345	LATDMGTMQErITTTKKGSIT
P69905|HBA_HUMAN	Hemoglobin subunit alpha OS=Homo sapiens OX=9606 GN=HBA1 PE=1 SV=2	R32	AGEYGAEALErMFLSFPTTKT
A5A3E0|POTEF_HUMAN	POTE ankyrin domain family member F OS=Homo sapiens OX=9606 GN=POTEF PE=1 SV=2	R762	SYVGKEAQSKrGILTLKYPME
P07900|HS90A_HUMAN	Heat shock protein HSP 90-alpha OS=Homo sapiens OX=9606 GN=HSP90AA1 PE=1 SV=5	R620	MERIMKAQALrDNSTMGYMAA
P25705|ATPA_HUMAN	ATP synthase subunit alpha mitochondrial OS=Homo sapiens OX=9606 GN=ATP5F1A PE=1 SV=1	R186	APGIIPRISVrEPMQTGIKAV
	ATP synthase subunit alpha mitochondrial OS=Homo sapiens OX=9606 GN=ATP5F1A PE=1 SV=1	R262	KRSTVAQLVKrLTDADAMKYT
P08238|HS90B_HUMAN	Heat shock protein HSP 90-beta OS=Homo sapiens OX=9606 GN=HSP90AB1 PE=1 SV=4	R291	ELNKTKPIWTrNPDDITQEEY
	Heat shock protein HSP 90-beta OS=Homo sapiens OX=9606 GN=HSP90AB1 PE=1 SV=4	R604	STYGWTANMErIMKAQALRDN
	Heat shock protein HSP 90-beta OS=Homo sapiens OX=9606 GN=HSP90AB1 PE=1 SV=4	R612	MERIMKAQALrDNSTMGYMMA
P31146|COR1A_HUMAN	Coronin-1A OS=Homo sapiens OX=9606 GN=CORO1A PE=1 SV=4	R354	RCEPIAMTVPrKSDLFQEDLY
	Coronin-1A OS=Homo sapiens OX=9606 GN=CORO1A PE=1 SV=4	R408	PPKSRELRVNrGLDTGRRRAA
	Coronin-1A OS=Homo sapiens OX=9606 GN=CORO1A PE=1 SV=4	R450	LQATVQELQKrLDRLEETVQA
Q13509|TBB3_HUMAN	Tubulin beta-3 chain OS=Homo sapiens OX=9606 GN=TUBB3 PE=1 SV=2	R2	*********MrEIVHIQAGQC
	Tubulin beta-3 chain OS=Homo sapiens OX=9606 GN=TUBB3 PE=1 SV=2	R121	ELVDSVLDVVrKECENCDCLQ

P22626|ROA2_HUMAN	Heterogeneous nuclear ribonucleoproteins A2/B1 OS=Homo sapiens OX=9606 GN=HNRNPA2B1 PE=1 SV=2	R200	RQEMQEVQSSrSGRGGNFGFG
	Heterogeneous nuclear ribonucleoproteins A2/B1 OS=Homo sapiens OX=9606 GN=HNRNPA2B1 PE=1 SV=2	R203	MQEVQSSRSGrGGNFGFGDSR
	Heterogeneous nuclear ribonucleoproteins A2/B1 OS=Homo sapiens OX=9606 GN=HNRNPA2B1 PE=1 SV=2	R228	NFGPGPGSNFrGGSDGYGSGR
P08133|ANXA6_HUMAN	Annexin A6 OS=Homo sapiens OX=9606 GN=ANXA6 PE=1 SV=3	R358	VARVELKGTVrPANDFNPDAD
P68104|EF1A1_HUMAN	Elongation factor 1-alpha 1 OS=Homo sapiens OX=9606 GN=EEF1A1 PE=1 SV=1	R423	ESFSDYPPLGrFAVRDMRQTV
Q03252|LMNB2_HUMAN	Lamin-B2 OS=Homo sapiens OX=9606 GN=LMNB2 PE=1 SV=4	R28	AATMATPLPGrAGGPATPLSP
P52272|HNRPM_HUMAN	Heterogeneous nuclear ribonucleoprotein M OS=Homo sapiens OX=9606 GN=HNRNPM PE=1 SV=3	R410	GIERMGPGIDrLGGAGMERMG
	Heterogeneous nuclear ribonucleoprotein M OS=Homo sapiens OX=9606 GN=HNRNPM PE=1 SV=3	R429	MGAGLGHGMDrVGSEIERMGL
	Heterogeneous nuclear ribonucleoprotein M OS=Homo sapiens OX=9606 GN=HNRNPM PE=1 SV=3	R443	EIERMGLVMDrMGSVERMGSG
P63104|1433Z_HUMAN	14-3-3 protein zeta/delta OS=Homo sapiens OX=9606 GN=YWHAZ PE=1 SV=1	R18	QKAKLAEQAErYDDMAACMKS
P60174|TPIS_HUMAN	Triosephosphate isomerase OS=Homo sapiens OX=9606 GN=TPI1 PE=1 SV=4	R53	APPTAYIDFArQKLDPKIAVA
P60660|MYL6_HUMAN	Myosin light polypeptide 6 OS=Homo sapiens OX=9606 GN=MYL6 PE=1 SV=2	R110	GNGTVMGAEIrHVLVTLGEKM
Q00610|CLH1_HUMAN	Clathrin heavy chain 1 OS=Homo sapiens OX=9606 GN=CLTC PE=1 SV=5	R1620	VDKLDASESLrKEEEQATETQ
Q93084|AT2A3_HUMAN	Sarcoplasmic/endoplasmic reticulum calcium ATPase 3 OS=Homo sapiens OX=9606 GN=ATP2A3 PE=1 SV=2	R164	AVGDKVPADLrLIEIKSTTLR
P22314|UBA1_HUMAN	Ubiquitin-like modifier-activating enzyme 1 OS=Homo sapiens OX=9606 GN=UBA1 PE=1 SV=3	R239	PGVVTCLDEArHGFESGDFVS

	Ubiquitin-like modifier-activating enzyme 1 OS=Homo sapiens OX=9606 GN=UBA1 PE=1 SV=3	R880	AENYDIPSADrHKSKLIAGKI
P52566|GDIR2_HUMAN	Rho GDP-dissociation inhibitor 2 OS=Homo sapiens OX=9606 GN=ARHGDIB PE=1 SV=3	R149	ATFMVGSYGPrPEEYEFLTPV
P61978|HNRPK_HUMAN	Heterogeneous nuclear ribonucleoprotein K OS=Homo sapiens OX=9606 GN=HNRNPK PE=1 SV=1	R37	MEEEQAFKRSrNTDEMVELRI
P08567|PLEK_HUMAN	Pleckstrin OS=Homo sapiens OX=9606 GN=PLEK PE=1 SV=3	R174	WLVSNQSVRNrQEGLMIASSL
	Pleckstrin OS=Homo sapiens OX=9606 GN=PLEK PE=1 SV=3	R307	VTSVESNSNGrKSEEENLFEI
P37802|TAGL2_HUMAN	Transgelin-2 OS=Homo sapiens OX=9606 GN=TAGLN2 PE=1 SV=3	R4	*******MANrGPAYGLSREV
	Transgelin-2 OS=Homo sapiens OX=9606 GN=TAGLN2 PE=1 SV=3	R196	QAGMTGYGMPrQIL*******
P61158|ARP3_HUMAN	Actin-related protein 3 OS=Homo sapiens OX=9606 GN=ACTR3 PE=1 SV=3	R4	*******MAGrLPACVVDCGT
P31946|1433B_HUMAN	14-3-3 protein beta/alpha OS=Homo sapiens OX=9606 GN=YWHAB PE=1 SV=3	R20	QKAKLAEQAErYDDMAAAMKA
P08311|CATG_HUMAN	Cathepsin G OS=Homo sapiens OX=9606 GN=CTSG PE=1 SV=2	R82	VTLGAHNIQRrENTQQHITAR
P02671|FIBA_HUMAN	Fibrinogen alpha chain OS=Homo sapiens OX=9606 GN=FGA PE=1 SV=2	R263	DMPQMRMELErPGGNEITRGG
	Fibrinogen alpha chain OS=Homo sapiens OX=9606 GN=FGA PE=1 SV=2	R512	GIGTLDGFRHrHPDEAAFFDT
P15311|EZRI_HUMAN	Ezrin OS=Homo sapiens OX=9606 GN=EZR PE=1 SV=4	R295	MGNHELYMRRrKPDTIEVQQM
Q9Y4G6|TLN2_HUMAN	Talin-2 OS=Homo sapiens OX=9606 GN=TLN2 PE=1 SV=4	R209	FFYSDQNVDSrDPVQLNLLYV
	Talin-2 OS=Homo sapiens OX=9606 GN=TLN2 PE=1 SV=4	R2198	AKAVAAGNSCrQEDVIATANL
P26599|PTBP1_HUMAN	Polypyrimidine tract-binding protein 1 OS=Homo sapiens OX=9606 GN=PTBP1 PE=1 SV=1	R254	QNIYNACCTLrIDFSKLTSLN
P02545|LMNA_HUMAN	Prelamin-A/C OS=Homo sapiens OX=9606 GN=LMNA PE=1 SV=1	R329	KLRDLEDSLArERDTSRRLLA
P41218|MNDA_HUMAN	Myeloid cell nuclear differentiation antigen OS=Homo sapiens OX=9606 GN=MNDA PE=1 SV=1	R204	TQAQRQVDARrNVPQNDPVTV
P23527|H2B1O_HUMAN	Histone H2B type 1-O OS=Homo sapiens OX=9606 GN=H2BC17 PE=1 SV=3	R93	HYNKRSTITSrEIQTAVRLLL

Q99879|H2B1M_HUMAN	Histone H2B type 1-M OS=Homo sapiens OX=9606 GN=H2BC14 PE=1 SV=3	R93	HYNKRSTITSrEIQTAVRLLL
Q93079|H2B1H_HUMAN	Histone H2B type 1-H OS=Homo sapiens OX=9606 GN=H2BC9 PE=1 SV=3	R93	HYNKRSTITSrEIQTAVRLLL
P33778|H2B1B_HUMAN	Histone H2B type 1-B OS=Homo sapiens OX=9606 GN=H2BC3 PE=1 SV=2	R93	HYNKRSTITSrEIQTAVRLLL
P06899|H2B1J_HUMAN	Histone H2B type 1-J OS=Homo sapiens OX=9606 GN=H2BC11 PE=1 SV=3	R93	HYNKRSTITSrEIQTAVRLLL
P58876|H2B1D_HUMAN	Histone H2B type 1-D OS=Homo sapiens OX=9606 GN=H2BC5 PE=1 SV=2	R93	HYNKRSTITSrEIQTAVRLLL
Q99877|H2B1N_HUMAN	Histone H2B type 1-N OS=Homo sapiens OX=9606 GN=H2BC15 PE=1 SV=3	R93	HYNKRSTITSrEIQTAVRLLL
O60814|H2B1K_HUMAN	Histone H2B type 1-K OS=Homo sapiens OX=9606 GN=H2BC12 PE=1 SV=3	R93	HYNKRSTITSrEIQTAVRLLL
P09382|LEG1_HUMAN	Galectin-1 OS=Homo sapiens OX=9606 GN=LGALS1 PE=1 SV=2	R21	NLKPGECLRVrGEVAPDAKSF
Q16181|SEPT7_HUMAN	Septin-7 OS=Homo sapiens OX=9606 GN=SEPTIN7 PE=1 SV=2	R425	QRILEQQNSSrTLEKNKKKGK
P61626|LYSC_HUMAN	Lysozyme C OS=Homo sapiens OX=9606 GN=LYZ PE=1 SV=1	R68	TRATNYNAGDrSTDYGIFQIN
P18669|PGAM1_HUMAN	Phosphoglycerate mutase 1 OS=Homo sapiens OX=9606 GN=PGAM1 PE=1 SV=2	R162	SCESLKDTIArALPFWNEEIV
Q9UGI8|TES_HUMAN	Testin OS=Homo sapiens OX=9606 GN=TES PE=1 SV=1	R254	KEGDPAIYAErAGYDKLWHPA
P47756|CAPZB_HUMAN	F-actin-capping protein subunit beta OS=Homo sapiens OX=9606 GN=CAPZB PE=1 SV=4	R15	QLDCALDLMRrLPPQQIEKNL
	F-actin-capping protein subunit beta OS=Homo sapiens OX=9606 GN=CAPZB PE=1 SV=4	R244	GKTKDIVNGLrSIDAIPDNQK
P62820|RAB1A_HUMAN	Ras-related protein Rab-1A OS=Homo sapiens OX=9606 GN=RAB1A PE=1 SV=3	R72	LQIWDTAGQErFRTITSSYYR
P52209|6PGD_HUMAN	6-phosphogluconate dehydrogenase decarboxylating OS=Homo sapiens OX=9606 GN=PGD PE=1 SV=3	R136	SGVSGGEEGArYGPSLMPGGN
Q13576|IQGA2_HUMAN	Ras GTPase-activating-like protein IQGAP2 OS=Homo sapiens OX=9606 GN=IQGAP2 PE=1 SV=4	R1342	EVDHATDMVSrAMIDSRTPEE
P19971|TYPH_HUMAN	Thymidine phosphorylase OS=Homo sapiens OX=9606 GN=TYMP PE=1	R265	LVGVGASLGLrVAAALTAMDK

	SV=2		
P61981|1433G_HUMAN	14-3-3 protein gamma OS=Homo sapiens OX=9606 GN=YWHAG PE=1 SV=2	R19	QKARLAEQAErYDDMAAAMKN
P61160|ARP2_HUMAN	Actin-related protein 2 OS=Homo sapiens OX=9606 GN=ACTR2 PE=1 SV=1	R80	VNYPMENGIVrNWDDMKHLWD
Q13418|ILK_HUMAN	Integrin-linked protein kinase OS=Homo sapiens OX=9606 GN=ILK PE=1 SV=2	R56	RSAVVEMLIMrGARINVMNRG
Q9H0U4|RAB1B_HUMAN	Ras-related protein Rab-1B OS=Homo sapiens OX=9606 GN=RAB1B PE=1 SV=1	R69	LQIWDTAGQErFRTITSSYYR
P09972|ALDOC_HUMAN	Fructose-bisphosphate aldolase C OS=Homo sapiens OX=9606 GN=ALDOC PE=1 SV=2	R201	ILPDGDHDLKrCQYVTEKVLA
Q15233|NONO_HUMAN	Non-POU domain-containing octamer-binding protein OS=Homo sapiens OX=9606 GN=NONO PE=1 SV=4	R202	IVEFSGKPAArKALDRCSEGS
Q13011|ECH1_HUMAN	Delta(3 5)-Delta(2 4)-dienoyl-CoA isomerase mitochondrial OS=Homo sapiens OX=9606 GN=ECH1 PE=1 SV=2	R59	EAPDHSYESLrVTSAQKHVLH
	Delta(3 5)-Delta(2 4)-dienoyl-CoA isomerase mitochondrial OS=Homo sapiens OX=9606 GN=ECH1 PE=1 SV=2	R245	DEALGSGLVSrVFPDKEVMLD
P04843|RPN1_HUMAN	Dolichyl-diphosphooligosaccharide--protein glycosyltransferase subunit 1 OS=Homo sapiens OX=9606 GN=RPN1 PE=1 SV=1	R65	LAHLGGGSTSrATSFLLALEP
P21281|VATB2_HUMAN	V-type proton ATPase subunit B brain isoform OS=Homo sapiens OX=9606 GN=ATP6V1B2 PE=1 SV=3	R185	SAIDGMNSIArGQKIPIFSAA
	V-type proton ATPase subunit B brain isoform OS=Homo sapiens OX=9606 GN=ATP6V1B2 PE=1 SV=3	R471	NFIAQGPYENrTVFETLDIGW
P61106|RAB14_HUMAN	Ras-related protein Rab-14 OS=Homo sapiens OX=9606 GN=RAB14 PE=1 SV=4	R72	LQIWDTAGQErFRAVTRSYYR
P27797|CALR_HUMAN	Calreticulin OS=Homo sapiens OX=9606 GN=CALR PE=1 SV=1	R162	GKNVLINKDIrCKDDEFTHLY
	Calreticulin OS=Homo sapiens OX=9606 GN=CALR PE=1 SV=1	R222	DASKPEDWDErAKIDDPTDSK

Q96AE4|FUBP1_HUMAN	Far upstream element-binding protein 1 OS=Homo sapiens OX=9606 GN=FUBP1 PE=1 SV=3	R271	FREVRNEYGSrIGGNEGIDVP
P35241|RADI_HUMAN	Radixin OS=Homo sapiens OX=9606 GN=RDX PE=1 SV=1	R295	MGNHELYMRRrKPDTIEVQQM
P14543|NID1_HUMAN	Nidogen-1 OS=Homo sapiens OX=9606 GN=NID1 PE=1 SV=3	R1017	LHGGEPTTIIrQDLGSPEGIA
P00491|PNPH_HUMAN	Purine nucleoside phosphorylase OS=Homo sapiens OX=9606 GN=PNP PE=1 SV=2	R229	MSTVPEVIVArHCGLRVFGFS
P02787|TRFE_HUMAN	Serotransferrin OS=Homo sapiens OX=9606 GN=TF PE=1 SV=3	R696	TSSLLEACTFrRP********
P84243|H33_HUMAN	Histone H3.3 OS=Homo sapiens OX=9606 GN=H3-3A PE=1 SV=2	R43	TGGVKKPHRYrPGTVALREIR
	Histone H3.3 OS=Homo sapiens OX=9606 GN=H3-3A PE=1 SV=2	R117	DTNLCAIHAKrVTIMPKDIQL
	Histone H3.2 OS=Homo sapiens OX=9606 GN=H3C15 PE=1 SV=3	R43	TGGVKKPHRYrPGTVALREIR
	Histone H3.2 OS=Homo sapiens OX=9606 GN=H3C15 PE=1 SV=3	R117	DTNLCAIHAKrVTIMPKDIQL
P59998|ARPC4_HUMAN	Actin-related protein 2/3 complex subunit 4 OS=Homo sapiens OX=9606 GN=ARPC4 PE=1 SV=3	R71	VLIEGSINSVrVSIAVKQADE
O00194|RB27B_HUMAN	Ras-related protein Rab-27B OS=Homo sapiens OX=9606 GN=RAB27B PE=1 SV=4	R80	LQLWDTAGQErFRSLTTAFFR
	Ras-related protein Rab-8A OS=Homo sapiens OX=9606 GN=RAB8A PE=1 SV=1	R69	LQIWDTAGQErFRTITTAYYR
P52565|GDIR1_HUMAN	Rho GDP-dissociation inhibitor 1 OS=Homo sapiens OX=9606 GN=ARHGDIA PE=1 SV=3	R172	VEEAPKGMLArGSYSIKSRFT
P35908|K22E_HUMAN	Keratin type II cytoskeletal 2 epidermal OS=Homo sapiens OX=9606 GN=KRT2 PE=1 SV=2	R430	VQDAIADAEQrGEHALKDARN
P05141|ADT2_HUMAN	ADP/ATP translocase 2 OS=Homo sapiens OX=9606 GN=SLC25A5 PE=1 SV=7	R259	IMYTGTLDCWrKIARDEGGKA
Q9NRW1|RAB6B_HUMAN	Ras-related protein Rab-6B OS=Homo sapiens OX=9606 GN=RAB6B PE=1 SV=1	R74	LQLWDTAGQErFRSLIPSYIR
Q96KP4|CNDP2_HUMAN	Cytosolic non-specific dipeptidase OS=Homo sapiens OX=9606 GN=CNDP2 PE=1 SV=2	R453	GAHSQNEKLNrYNYIEGTKML

P46459|NSF_HUMAN	Vesicle-fusing ATPase OS=Homo sapiens OX=9606 GN=NSF PE=1 SV=3	R67	PGSIAFSLPQrKWAGLSIGQE
	Vesicle-fusing ATPase OS=Homo sapiens OX=9606 GN=NSF PE=1 SV=3	R533	LLVQQTKNSDrTPLVSVLLEG
P20340|RAB6A_HUMAN	Ras-related protein Rab-6A OS=Homo sapiens OX=9606 GN=RAB6A PE=1 SV=3	R74	LQLWDTAGQErFRSLIPSYIR
P62491|RB11A_HUMAN	Ras-related protein Rab-11A OS=Homo sapiens OX=9606 GN=RAB11A PE=1 SV=3	R33	GKSNLLSRFTrNEFNLESKST
P49748|ACADV_HUMAN	Very long-chain specific acyl-CoA dehydrogenase mitochondrial OS=Homo sapiens OX=9606 GN=ACADVL PE=1 SV=1	R229	PSSGSDAASIrTSAVPSPCGK
P14222|PERF_HUMAN	Perforin-1 OS=Homo sapiens OX=9606 GN=PRF1 PE=1 SV=1	R177	YSFSTDTVECrFYSFHVVHTP
Q13126|MTAP_HUMAN	S-methyl-5'-thioadenosine phosphorylase OS=Homo sapiens OX=9606 GN=MTAP PE=1 SV=2	R133	SFYDGSHSCArGVCHIPMAEP
P09486|SPRC_HUMAN	SPARC OS=Homo sapiens OX=9606 GN=SPARC PE=1 SV=1	R205	RVKKIHENEKrLEAGDHPVEL
P61026|RAB10_HUMAN	Ras-related protein Rab-10 OS=Homo sapiens OX=9606 GN=RAB10 PE=1 SV=1	R70	LQIWDTAGQErFHTITTSYYR
O14983|AT2A1_HUMAN	Sarcoplasmic/endoplasmic reticulum calcium ATPase 1 OS=Homo sapiens OX=9606 GN=ATP2A1 PE=1 SV=1	R164	AVGDKVPADIrILAIKSTTLR
P54577|SYYC_HUMAN	Tyrosine--tRNA ligase cytoplasmic OS=Homo sapiens OX=9606 GN=YARS1 PE=1 SV=4	R207	KYLPALGYSKrVHLMNPMVPG
P49821|NDUV1_HUMAN	NADH dehydrogenase [ubiquinone] flavoprotein 1 mitochondrial OS=Homo sapiens OX=9606 GN=NDUFV1 PE=1 SV=4	R256	ETVAVSPTICrRGGTWFAGFG
Q92930|RAB8B_HUMAN	Ras-related protein Rab-8B OS=Homo sapiens OX=9606 GN=RAB8B PE=1 SV=2	R69	LQIWDTAGQErFRTITTAYYR
O43488|ARK72_HUMAN	Aflatoxin B1 aldehyde reductase member 2 OS=Homo sapiens OX=9606 GN=AKR7A2 PE=1 SV=3	R61	MDAPASAAAVrAFLERGHTEL
O14974|MYPT1_HUMAN	Protein phosphatase 1 regulatory subunit 12A OS=Homo sapiens OX=9606 GN=PPP1R12A PE=1 SV=1	R31	ETDLEPPVVKrQKTKVKFDDG

P51159|RB27A_HUMAN	Ras-related protein Rab-27A OS=Homo sapiens OX=9606 GN=RAB27A PE=1 SV=3	R80	LQLWDTAGQErFRSLTTAFFR
P25325|THTM_HUMAN	3-mercaptopyruvate sulfurtransferase OS=Homo sapiens OX=9606 GN=MPST PE=1 SV=3	R137	LLDGGLRHWLrQNLPLSSGKS
P30038|AL4A1_HUMAN	Delta-1-pyrroline-5-carboxylate dehydrogenase mitochondrial OS=Homo sapiens OX=9606 GN=ALDH4A1 PE=1 SV=3	R338	DVESVVSGTLrSAFEYGGQKC
Q8NF50|DOCK8_HUMAN	Dedicator of cytokinesis protein 8 OS=Homo sapiens OX=9606 GN=DOCK8 PE=1 SV=3	R1358	KVSTQVLQKSrDVKARLEEAL
Q14166|TTL12_HUMAN	Tubulin--tyrosine ligase-like protein 12 OS=Homo sapiens OX=9606 GN=TTLL12 PE=1 SV=2	R461	KYIESPVLFLrEDVGKVKFDI
P62753|RS6_HUMAN	40S ribosomal protein S6 OS=Homo sapiens OX=9606 GN=RPS6 PE=1 SV=1	R51	LGEEWKGYVVrISGGNDKQGF
Q15286|RAB35_HUMAN	Ras-related protein Rab-35 OS=Homo sapiens OX=9606 GN=RAB35 PE=1 SV=1	R69	LQIWDTAGQErFRTITSTYYR
Q02878|RL6_HUMAN	60S ribosomal protein L6 OS=Homo sapiens OX=9606 GN=RPL6 PE=1 SV=3	R105	PVGGDKNGGTrVVKLRKMPRY
P25098|ARBK1_HUMAN	Beta-adrenergic receptor kinase 1 OS=Homo sapiens OX=9606 GN=GRK2 PE=1 SV=2	R454	AQEVKESPFFrSLDWQMVFLQ
Q14558|KPRA_HUMAN	Phosphoribosyl pyrophosphate synthase-associated protein 1 OS=Homo sapiens OX=9606 GN=PRPSAP1 PE=1 SV=2	R295	THGILSAEAPrLIEESSVDEV
O95716|RAB3D_HUMAN	Ras-related protein Rab-3D OS=Homo sapiens OX=9606 GN=RAB3D PE=1 SV=1	R83	LQIWDTAGQErYRTITTAYYR
P11217|PYGM_HUMAN	Glycogen phosphorylase muscle form OS=Homo sapiens OX=9606 GN=PYGM PE=1 SV=6	R17	DQEKRKQISVrGLAGVENVTE
P61018|RAB4B_HUMAN	Ras-related protein Rab-4B OS=Homo sapiens OX=9606 GN=RAB4B PE=1 SV=1	R69	LQIWDTAGQErFRSVTRSYYR
Q96E17|RAB3C_HUMAN	Ras-related protein Rab-3C OS=Homo sapiens OX=9606 GN=RAB3C PE=1 SV=1	R91	LQIWDTAGQErYRTITTAYYR

Q96AX2|RAB37_HUMAN	Ras-related protein Rab-37 OS=Homo sapiens OX=9606 GN=RAB37 PE=1 SV=3	R91	LQIWDTAGQErFRSVTHAYYR
Q9Y2Z0|SGT1_HUMAN	Protein SGT1 homolog OS=Homo sapiens OX=9606 GN=SUGT1 PE=1 SV=3	R84	LNPNNSTAMLrKGICEYHEKN
Q96GD0|PLPP_HUMAN	Pyridoxal phosphate phosphatase OS=Homo sapiens OX=9606 GN=PDXP PE=1 SV=2	R142	DPSAGDGAAPrVRAVLVGYDE
Q13501|SQSTM_HUMAN	Sequestosome-1 OS=Homo sapiens OX=9606 GN=SQSTM1 PE=1 SV=1	R217	SPRPPRAGEArPGPTAESASG
Q86YS6|RAB43_HUMAN	Ras-related protein Rab-43 OS=Homo sapiens OX=9606 GN=RAB43 PE=1 SV=1	R79	LQIWDTAGQErFRTITQSYYR
P14174|MIF_HUMAN	Macrophage migration inhibitory factor OS=Homo sapiens OX=9606 GN=MIF PE=1 SV=4	R12	PMFIVNTNVPrASVPDGFLSE
P20337|RAB3B_HUMAN	Ras-related protein Rab-3B OS=Homo sapiens OX=9606 GN=RAB3B PE=1 SV=2	R83	LQIWDTAGQErYRTITTAYYR
Q7Z6P3|RAB44_HUMAN	Ras-related protein Rab-44 OS=Homo sapiens OX=9606 GN=RAB44 PE=1 SV=4	R894	LQLWDTAGQErYHSMTRQLLR
Q9BWS9|CHID1_HUMAN	Chitinase domain-containing protein 1 OS=Homo sapiens OX=9606 GN=CHID1 PE=1 SV=1	R65	LKAESVVLEHrSYCSAKARDR
Q16658|FSCN1_HUMAN	Fascin OS=Homo sapiens OX=9606 GN=FSCN1 PE=1 SV=3	R205	FLRHDGRLVArPEPATGYTLE
P02749|APOH_HUMAN	Beta-2-glycoprotein 1 OS=Homo sapiens OX=9606 GN=APOH PE=1 SV=3	R96	FAGILENGAVrYTTFEYPNTI
Q0VD83|APOBR_HUMAN	Apolipoprotein B receptor OS=Homo sapiens OX=9606 GN=APOBR PE=1 SV=3	R928	DAEGLMVTGGrRAEAKETEPE
P35250|RFC2_HUMAN	Replication factor C subunit 2 OS=Homo sapiens OX=9606 GN=RFC2 PE=1 SV=3	R155	SMTDGAQQALrRTMEIYSKTT
Q9HBH5|RDH14_HUMAN	Retinol dehydrogenase 14 OS=Homo sapiens OX=9606 GN=RDH14 PE=1 SV=1	R234	NILFTRELARrLEGTNVTVNV
P07478|TRY2_HUMAN	Trypsin-2 OS=Homo sapiens OX=9606 GN=PRSS2 PE=1 SV=1	R122	KLSSPAVINSrVSAISLPTAP
Q8TBH0|ARRD2_HUMAN	Arrestin domain-containing protein 2 OS=Homo sapiens OX=9606 GN=ARRDC2 PE=1 SV=2	R43	RVLLELSSAArVGALRLRARG

Q8WY91|THAP4_HUMAN	Peroxynitrite isomerase THAP4 OS=Homo sapiens OX=9606 GN=THAP4 PE=1 SV=2	R156	QAALQGEATPrAAQEAASQEQ
Q8IVF5|TIAM2_HUMAN	T-lymphoma invasion and metastasis-inducing protein 2 OS=Homo sapiens OX=9606 GN=TIAM2 PE=2 SV=4	R1655	DRGTLLKAQIrHQSLDSQSEN
Q92618|ZN516_HUMAN	Zinc finger protein 516 OS=Homo sapiens OX=9606 GN=ZNF516 PE=1 SV=1	R1086	WGVSGPGLEHrGTLRTQARPG
P98160|PGBM_HUMAN	Basement membrane-specific heparan sulfate proteoglycan core protein OS=Homo sapiens OX=9606 GN=HSPG2 PE=1 SV=4	R2655	QTLDLNCVVArQPQAIITWYK
Q86SX3|TEDC1_HUMAN	Tubulin epsilon and delta complex protein 1 OS=Homo sapiens OX=9606 GN=TEDC1 PE=1 SV=2	R257	HSFCTPGMGPrTFWNDLWLVC
A3KMH1|VWA8_HUMAN	von Willebrand factor A domain-containing protein 8 OS=Homo sapiens OX=9606 GN=VWA8 PE=1 SV=2	R1259	SLTVLDVLEGrTHTISLPINL
Q14993|COJA1_HUMAN	Collagen alpha-1(XIX) chain OS=Homo sapiens OX=9606 GN=COL19A1 PE=1 SV=3	R27	LLPASTSVTVrDKTEESCPIL
Q6ZRP7|QSOX2_HUMAN	Sulfhydryl oxidase 2 OS=Homo sapiens OX=9606 GN=QSOX2 PE=1 SV=3	R109	PTWRALAGDVrDWASAIRVAA
A6NI79|CCD69_HUMAN	Coiled-coil domain-containing protein 69 OS=Homo sapiens OX=9606 GN=CCDC69 PE=1 SV=1	R271	LQQEKEELLYrVLGANASPAF
O15409|FOXP2_HUMAN	Forkhead box protein P2 OS=Homo sapiens OX=9606 GN=FOXP2 PE=1 SV=2	R382	ALDDRSTAQCrVQMQVVQQLE

GRAPHICAL ABSTRACT